

POLITECNICO OF TURIN

Course in Master's Degree in  
Automotive Engineering

Master's Degree Thesis

Design of engine components with thermoplastic composite material:  
Wrist Pin



**Relator/Correlator**

prof. Paolo Baldissera  
prof. Cristiana Delprete

**Candidate**

Giuseppe La Placa

A.Y. 2018/2019

## **Abstract**

The twenty-first century was characterized by an increasing demand in terms of technology progress, from the informatic field to the automotive one. Regarding the automotive field, in the last years global pollution became more and more important and, with this in mind the engine efficiency and the fuel saving have concentrated on themselves the efforts of the fabricants.

The project is based on the usage of composite materials in the automotive field. In order to reach this goal, FEM (Finite Element Method) analyzes have been performed on different engine components. In particular, this project focus on the wrist pin, between the piston and the connecting rod. A parallel study was made on the connecting rod, following the same physical model.

The original geometry of the components comes from a FIAT Fire 1.4 8V engine. The new components have been redesigned coherently with the composite material properties in order to be produced and to resist to the stress due to combustion. The aim of the new design is to produce the components with the actual technologies. The use of composite materials allows to reduce considerably the weight of the components and therefore the inertial forces on the engine. However, the aim of this project is not only to reduce weight, but also to design an optimal fibers orientation. In this way it is possible to avoid discharged portion of material inside the component.

To perform the FEM analysis, different programs have been used. First, the geometry of the pin was drawn on Solidworks. Then the pin was meshed with Altair Hypermesh. The simulation was performed with the solver Altair Optistruct. Finally, the results were analyzed with the post-processing software Altair Hyperview.

During the preparation of the model, a new feature of Hypermesh was used. It is the PCOMPLS property, a particular property able to simulate solid composite layers. Usually, composite materials are analyzed with the Laminate Tool in Hypermesh. This tool is able to generate only shell elements, so surface elements, not suitable for this project. The tool was used as first attempt for the analysis, then PCOMPLS property was used. The characteristic of this property will be discussed later, as well as the laminate tool model preparation.

In order to converge the results of Optistruct, some modifications have been performed on the model, and will be discussed in the Model chapter. The divergence is due to the non-linearity of the analysis, due in turn to the introduction of contact surfaces between the different parts.

**Keywords:** *Composite Material, FEM Analysis, Hypermesh, Optistruct, Wrist Pin, Carbon Fiber*

## Table Of Contents

Abstract.....	I
Table Of Contents .....	II
List of Figures .....	IV
List of Tables .....	VII
List of Equations.....	VIII
I. Introduction.....	1
I. 1. General Introduction.....	1
I. 2. State of Art .....	1
I.1) 1. Current situation .....	1
I. 3. Objectives .....	2
I. 4. Composite Materials.....	2
I.4) 1. Why using composite materials? .....	3
I.4) 2. Why using orthotropic material? .....	3
II. Wrist Pin Analysis .....	4
II. 1. Wrist Pin Model - First Design.....	4
II. 2. Actual Model .....	5
II.2) 1. Steel Pin .....	5
II.2) 2. Composite Pin .....	5
II. 3. Maximum Compressive Force due to the Gas Pressure.....	6
III. Connecting Rod Analysis .....	8
III. 1. Steel Connecting Rod .....	8
III.1) 1. Geometrical Parameters .....	8
III.1) 2. Equivalent Crank Mechanism .....	9
III.1) 3. Evaluation of the Alternating Forces .....	9
III.1) 4. Evaluation of the Centrifugal Force .....	11
III. 2. Composite Connecting Rod.....	12
III.2) 1. Alternating Mass for Composite Material.....	12
III.2) 2. Centrifugal Force for Composite Material.....	12
III. 3. Results and Comparison between Steel and Composite .....	13
IV. Analysis Method.....	16
IV. 1. Geometry Models.....	16
IV. 2. Altair Hypermesh.....	17
IV.2) 1. Altair Hypermesh – Layered Shell using Laminate Tool.....	17

IV.2) 2.	Altair Hypermesh – Layered Solid Shell using PCOMPLS .....	22
IV.2) 3.	Altair Hypermesh – Layered Solid Shell using PSOLID .....	31
IV. 3.	Tsai-Wu Failure Criterion.....	33
V.	Conclusions .....	37
V. 1.	Consequences on engine .....	37
V. 2.	FEM Results .....	38
V.2) 1.	Laminated Wrist Pin .....	38
V.2) 2.	PCOMPLS Solid Layer Wrist Pin.....	43
V.2) 3.	PSOLID Solid Layer Wrist Pin .....	48
V.2) 4.	Comparison between PCOMPLS and PSOLID .....	52
V. 3.	Future developments.....	58
VI.	Bibliography.....	59

## List of Figures

Figure II. 1-1 Distributed Loaded Pin and Equivalent Model.....	4
Figure II. 1-2 Pin Geometry .....	5
Figure II. 3-1 Gas Pressure Trend.....	6
Figure II. 3-2 Gas Pressure Force .....	7
Figure III. 1-1 Reduced Connecting Rod.....	9
Figure III. 1-2 Centered Crank Mechanism Layout.....	10
Figure III. 1-3 Crank mass reduction.....	11
Figure III. 3-1 Alternating Forces Comparison.....	13
Figure III. 3-2 Torque Comparison at the crankshaft .....	14
Figure III. 3-3 Total Force Comparison between Steel and Composite.....	15
Figure IV. 1-1 APM Model.....	16
Figure IV. 1-2 SCPM Model.....	17
Figure IV. 2-1 PCOMPP Property Card.....	18
Figure IV. 2-2 Laminate Tool.....	18
Figure IV. 2-3 MAT8 Material Card .....	19
Figure IV. 2-4 Laminate Model .....	19
Figure IV. 2-5 Laminate Model with loads.....	20
Figure IV. 2-6 Laminate Model Results .....	21
Figure IV. 2-7 Complete Laminated Component Model.....	22
Figure IV. 2-8 MAT9ORT Material card.....	22
Figure IV. 2-9 PCOMPLS Reference System .....	23
Figure IV. 2-10 PCOMPLS Property Card .....	24
Figure IV. 2-11 Manual variation of the THETA by using .fem file .....	25
Figure IV. 2-12 PCOMPLS Reference system in the model.....	25
Figure IV. 2-13 Contact surfaces.....	26
Figure IV. 2-14 Contact groups .....	27
Figure IV. 2-15 PCOMPLS Supports Constraints.....	28
Figure IV. 2-16 Supports on the reduced connecting rod.....	29
Figure IV. 2-17 Constraint on RBE2 element .....	29
Figure IV. 2-18 Force and Support on RBE2.....	30
Figure IV. 2-19 Load Factors.....	30
Figure IV. 2-20 Script Opening .....	31
Figure IV. 2-21 Selection of the element.....	31
Figure IV. 2-22 Rotation of the fiber of the single element.....	32
Figure IV. 2-23 Fiber alignment for the attached mesh.....	32
Figure IV. 2-24 Material Orientation through "Systems" subpanel(*).....	32
Figure IV. 3-1 Tsai-Wu ellipse.....	35
Figure V. 1-1 Engine Block Forces .....	37
Figure V. 2-1 Principal Stress Directions .....	38
Figure V. 2-2 Laminated Pin Displacement Lateral View .....	39
Figure V. 2-3 Laminated Pin Displacement Top View.....	39
Figure V. 2-4 Laminated Pin Principal Stress Direction 1 Top View.....	40
Figure V. 2-5 Laminated Pin Principal Stress Direction 1 Bottom View .....	40

Figure V. 2-6 Laminated Pin Principal Stress Direction 3 Top View .....	41
Figure V. 2-7 Laminated Pin Principal Stress Direction 3 Bottom View .....	41
Figure V. 2-8 Laminated Pin Shear Stress Top View .....	42
Figure V. 2-9 Laminated Pin Shear Stress Bottom View .....	42
Figure V. 2-10 Laminated Pin Failure Index Top View .....	42
Figure V. 2-11 Laminated Pin Failure Index Bottom View .....	42
Figure V. 2-12 PCOMPLS Wrist Pin Displacement Lateral View .....	43
Figure V. 2-13 PCOMPLS Wrist Pin Displacement Top View .....	43
Figure V. 2-14 PCOMPLS Wrist Pin Displacement Lateral View after Load Application .....	44
Figure V. 2-15 PCOMPLS Pin Principal Stress Direction 1 Top View - Maximum Layer .....	45
Figure V. 2-16 PCOMPLS Pin Principal Stress Direction 1 Bottom View - Maximum Layer .....	45
Figure V. 2-17 PCOMPLS Pin Principal Stress Direction 2 Top View - Minimum Layer .....	46
Figure V. 2-18 PCOMPLS Pin Principal Stress Direction 2 Bottom View - Minimum Layer .....	46
Figure V. 2-19 PCOMPLS Pin Principal Stress Direction 3 Top View - Minimum Layer .....	47
Figure V. 2-20 PCOMPLS Pin Principal Stress Direction 3 Bottom View - Minimum Layer .....	47
Figure V. 2-21 PCOMPLS Pin Shear Stress Top View - Maximum Layer .....	48
Figure V. 2-22 PCOMPLS Pin Shear Stress Bottom View - Maximum Layer .....	48
Figure V. 2-23 PSOLID Wrist Pin Displacement Lateral View after Load Application .....	49
Figure V. 2-24 PSOLID Wrist Pin Displacement Top View .....	49
Figure V. 2-25 PSOLID Wrist Pin Displacement Lateral View after Load Application .....	49
Figure V. 2-26 PSOLID Pin Principal Stress Direction 1 Top View .....	50
Figure V. 2-27 PSOLID Pin Principal Stress Direction 1 Bottom View .....	50
Figure V. 2-28 PSOLID Pin Principal Stress Direction 2 Top View .....	50
Figure V. 2-29 PSOLID Pin Principal Stress Direction 2 Bottom View .....	51
Figure V. 2-30 PSOLID Pin Principal Stress Direction 3 Top View .....	51
Figure V. 2-31 PSOLID Pin Principal Stress Direction 3 Bottom View .....	51
Figure V. 2-32 PSOLID Pin Shear Stress Top View .....	52
Figure V. 2-33 PSOLID Pin Shear Stress Bottom View .....	52
Figure V. 2-34 Displacements Comparison Top View .....	53
Figure V. 2-35 Displacements Comparison Lateral View .....	53
Figure V. 2-36 Principal Stress Direction 1 Comparison Top View .....	54
Figure V. 2-37 Principal Stress Direction 1 Comparison Bottom View .....	54
Figure V. 2-38 Principal Stress Direction 2 Comparison Top View .....	55
Figure V. 2-39 Principal Stress Direction 2 Comparison Bottom View .....	55
Figure V. 2-40 Principal Stress Direction 3 Comparison Top View .....	55
Figure V. 2-41 Principal Stress Direction 3 Comparison Bottom View .....	56

Figure V. 2-42 Shear Stress Comparison Top View.....56  
Figure V. 2-43 Shear Stress Comparison Bottom View .....56

## **List f Tables**

Table I. 4-1 PEI-AS4 Mechanical Properties .....	3
Table III. 1-1 Geometrical Parameters.....	8
Table III. 1-2 Reduced Connecting Rod in Steel.....	9
Table III. 1-3 Reduced Conrod Masses (Steel) .....	9
Table III. 2-1 Mass Comparison .....	12
Table III. 2-2 Big Eye and Small Eye.....	12
Table III. 2-3 Rotating Mass and Force for Composite Components.....	12
Table III. 3-1 Maximum Compression Force Comparison .....	13
Table III. 3-2 Maximum Traction Force Comparison .....	13
Table IV. 2-1 PCOMPLS Format.....	22
Table IV. 2-2 PCOMPLS Details .....	23
Table IV. 3-1 Material Strengths.....	33
Table V. 1-1 Engine Block Forces Comparison.....	38

## **List of Equations**

Equation I. 4-1 Relation between Young Modulus, Shear Modulus and Poisson Coefficient.....	3
Equation II. 1-1 Wrist Pin First Design.....	5
Equation II. 2-1 Wrist Pin Actual Geometry.....	5
Equation III. 1-1 Geometrical Ratio.....	9
Equation III. 1-2 Piston Surface .....	9
Equation III. 1-3 Alternating Mass for Steel Conrod .....	10
Equation III. 1-4 Alternating Inertial Force.....	10
Equation III. 1-5 Maximum Rotational Speed .....	10
Equation III. 1-6 Centrifugal Force.....	11
Equation III. 1-7 Rotating Mass.....	11
Equation III. 1-8 Reduced Crank Web Mass .....	11
Equation III. 1-9 Rotating Mass for Steel Components .....	11
Equation III. 1-10 Centrifugal Force for Steel Components .....	11
Equation III. 2-1 Composite Alternating Mass.....	12
Equation III. 3-1 Cylinder Block Torque.....	14
Equation III. 3-2 Resultant Force on Crank Mechanism .....	14
Equation III. 3-3 Total Force acting on the Pin.....	14
Equation IV. 2-1 Ply Thickness Evaluation .....	23
Equation IV. 3-1 Tsai-Wu Failure Criterion.....	33
Equation IV. 3-2 Tsai-Wu Complete Failure Criterion .....	34
Equation IV. 3-3 Tsai-Wu Failure Coefficients.....	34
Equation IV. 3-4 Tsai-Wu Reduced Failure Criterion.....	34
Equation IV. 3-5 Tsai-Wu Reduced Criterion critical condition.....	34
Equation IV. 3-6 $F_{12}$ Critical Condition.....	34
Equation IV. 3-7 $F_{12}$ Evaluation .....	35
Equation V. 1-1 Engine Block Forces .....	37
Equation V. 2-1 Longitudinal Compressive Resistance.....	54
Equation V. 2-2 Transversal Compressive Resistance .....	55

## **I. Introduction**

### **I. 1. General Introduction**

The automotive industry is in continuous growth. New advances and stricter norms that affect the sector force the companies to develop and improve new technologies and studies to be competitive.

An increasing interest in the environment is characterizing the twenty-first century. Stringent rules force companies to produce more and more efficient engines in order to reduce pollutant emissions. With this perspective, companies are trying to update their technology.

Different “automotive factors” are still in development, from the aerodynamic efficiency, to the combustion improvement, until the reduction of the engine weight. In the latter this project is focused.

The usage of composite material in the engine, instead of conventional metal, allows a reduction up to 25% of the weight. This reduction has a positive impact on the whole engine structure. Indeed, a reduction of the components weight causes a reduction of the inertial forces. In turn, this reduction causes a more balanced engine in terms of vibrations. In this way it is possible to optimize the design of the entire powertrain system, from the crankshaft to the engine supports. It also increases the comfort perceived by the passengers, increasing the vehicle quality level.

Finite Element Method analysis is the most used analysis in terms of structural analysis. It makes possible to predict the behavior of a component before it is produced. FEM analysis allows to pre-design a component, characterize its behavior and modify it to be as much realistic as possible.

FEM analysis is very accurate and complex, giving the possibility to modify any parameter of the model. In this way it is possible to study separately all the different effects of each parameter involved, such as the mesh, the boundary conditions and the contacts between the different parts.

### **I. 2. State of Art**

#### **I.1) 1. Current situation**

The wrist pin is the connecting element between the piston and the connecting rod. Its geometry is a hollow cylinder with tapered ends and thicker in the middle. It is inserted into the piston hubs, passes through the small eye of the connecting rod and it is kept in position by using snap elastic rings inserted into the grooves of the piston hubs (relative motion occurs between pin and small eye and between pin and piston) or by using a screw (relative motion occurs only between pin and small eye).

It can assume two configurations:

- a. **Fixed pin**, in which the pin is fixed with respect to the small eye (on low stressed engine);
- b. **Floating pin**, in which the pin is free to rotate with respect the connecting rod by means of bushing or needle bearing (on medium/high stressed engine).

Actually the most used materials are those having high fatigue resistance and good surface hardness, such as NiCr and CrMn steels (e.g. 17Cr3, 16MnCr5) with UTS (Rm) up to 1500 MPa and hardness up to 240 HB (medium stressed engines) or CrMo and CrNiMo steels (e.g. 34NiCrMo16, 31CrMoV9) with hardness up to 270 HB (high stressed engines).

In order to reduce the reciprocating masses, composite material pin have been proposed. Details about the material used in this project will be discussed in the next paragraph.

### I. 3. Objectives

This project sets itself to face all the calculation about forces and torque on components and engine. Particular attention will be put on each force equation, in order to be clear and make possible to replicate all the calculations.

FEM analysis has been carried out in order to estimate the stresses and the strains along the components. The starting point for the FEM will be a rough model, in which the pin was studied alone. Finally, a more-and-more complete model will be set.

### I. 4. Composite Materials

A composite material is a material formed by combining two or more materials with significant differences in physical or chemical properties. In the engineering field there are many types of composite materials. This thesis is based on the "Laminated Composites", which are materials made up of any number of layered materials, of the same of different orientation, bonded together with a matrix material.

The choice for the work has fallen on a balanced composite material, the PEI-AS4. This material is the most suitable since its properties are really good in the interested directions and it is able to resist even at higher temperatures (almost 150°C). This allows to use it not only for the connecting rod, which is essentially loaded in one direction (the connecting rod direction itself), but also for the wrist pin.

The mechanical properties of the material are shown in the table:

<b>Young Modulus</b>	<b>E<sub>11</sub></b>	128700 MPa
	<b>E<sub>22</sub></b>	7600 MPa
	<b>E<sub>33</sub></b>	7600 MPa
<b>Shear Modulus</b>	<b>G<sub>12</sub></b>	4800 MPa
	<b>G<sub>13</sub></b>	4800 MPa
	<b>G<sub>23</sub></b>	2968, 75 MPa

<b>Maximum longitudinal stress</b>	<b>F<sub>1t</sub></b>	2176 MPa
<b>Maximum transversal stress</b>	<b>F<sub>2t</sub></b>	46,7 MPa
<b>Maximum shear stress</b>	<b>F<sub>6</sub></b>	140 MPa
<b>Material Density</b>	<b>ρ</b>	1,55 g/cm <sup>3</sup>
<b>Poisson coefficient</b>	<b>v<sub>12</sub></b>	0,28
	<b>v<sub>23</sub></b>	0,28
<b>Filling percentage</b>	<b>V<sub>f</sub></b>	55%

Table I. 4-1 PEI-AS4 Mechanical Properties

In the table is also showed the value of filling percentage, which represent the amount of fibers in percentage with respect to the matrix material. Higher V<sub>f</sub> can be achieved, but values above 55% lead to a considerably reduction of the laminate's mechanical properties.

The values showed in Table I. 4-1 are related each other according to following equation:

$$G_{ij} = \frac{E_{ii}}{2(1 + \nu_{ij})} \quad \text{with } i=1, 2, 3 \text{ and } j=1, 2, 3$$

Equation I. 4-1 Relation between Young Modulus, Shear Modulus and Poisson Coefficient

#### I.4) 1. Why using composite materials?

The material property of the composites can be engineered as per the application requirements as in this study case, in which there were different layering options. Composite materials property can be imparted giving them great advantage when compared with traditional homogeneous materials like steel or aluminum. Finally, composites have increased strength to weight ratios in use cases against isotropic metals.

For these reasons, applications like aerospace components, where the weight is a decisive factor, can benefit tremendously with the usage of composite materials.

Drawbacks:

1. Higher cost
2. Limited supply of raw materials
3. Complex manufacturing needs

Considering the automotive field, an engine is subjected to high loads deriving from the combustion and the inertial forces of the components. The original engine was endowed with steel connecting rod and wrist pin. Analyzing the resultant force acting on the engine block with all steel components (the calculation will be discussed in the paragraph V. 1. Consequences on engine), it is possible to notice that the value roams around 24 KN. Just by substituting the steel connecting rod and the wrist pin with those of composites, the reduction on the resultant force is about the 22% (18,5 KN).

#### I.4) 2. Why using orthotropic material?

Orthotropic materials' properties are the same in each of three orthogonal planes at a given point within a body. Thus, the material properties are dependent on orientation at a specified point within the body.

The next paragraph will show the steps used for the calculation of the forces and of the involved masses.

## II. Wrist Pin Analysis

### II. 1. Wrist Pin Model - First Design

As a first attempt the wrist pin is usually modeled as a supported beam loaded with distributed forces. The model is equivalent to a beam supported at the ends by one hinge and one support. It is loaded by three concentrated forces equivalent to the uniform distributed ones.

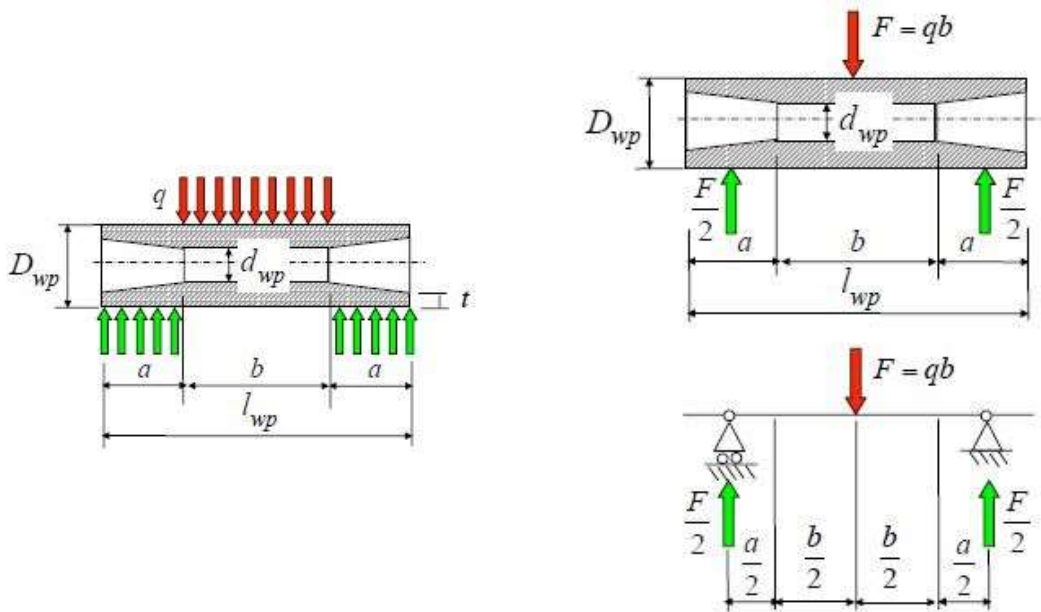


Figure II. 1-1 Distributed Loaded Pin and Equivalent Model

The value of the force depends on the type of calculation:

**Static:** this is the initial condition when the maximum torque regime is established. The value of the maximum compressive force due to the gas is taken and the inertial forces are neglected. This regime will be the one used for the FEM simulations;

**Fatigue:** this condition happens at the Top Dead Center (TDC) at the maximum spin speed regime. In this case the value of the force for the fatigue cycle is taken as the maximum value between the maximum gas force and the maximum inertial force.

The initial geometry of the pin is evaluated as follow:

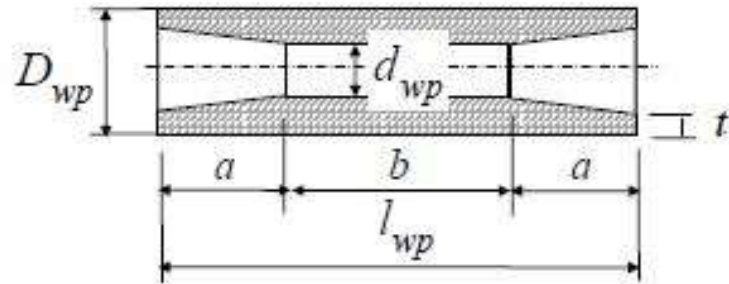


Figure II. 1-2 Pin Geometry

The length of the pin  $l_{wp}$  is assumed equal to the piston bore  $D$ . Pin outer diameter  $D_{wp}$  is initially assumed equal to the 35% of the bore. The inner diameter  $d_{wp}$  is equal to the 40% of the outer diameter. Finally, the minimum thickness  $t$  is equal to the 50% of the inner diameter

$$\begin{cases} D_{wp} = 0.35 D \\ d_{wp} = 0.40 D_{wp} = 0.14 D \\ t = 0.50 d_{wp} = 0.07 D \end{cases}$$

Equation II. 1-1 Wrist Pin First Design

## II. 2. Actual Model

Once the general model definition is given, it is necessary to introduce the actual model. The model just explained showed the way in which the first design of the wrist pin is done. In this case, the engine was already designed. So the starting geometry was the original one taken from the engine itself. The internal surface of the wrist pin is not tapered, differently from what is shown in Figure II. 1-2 Pin Geometry.

### II.2) 1. Steel Pin

First, the analysis was conducted on the original steel pin. The geometry of the wrist pin is shown in the following equation:

$$\begin{cases} D_{wp} = 18 \text{ mm} \\ d_{wp} = 6 \text{ mm} \\ t = 6 \text{ mm} \end{cases}$$

Equation II. 2-1 Wrist Pin Actual Geometry

The mass properties have been assigned into Solidworks and the mass value for the steel wrist pin was 72g.

### II.2) 2. Composite Pin

Next, maintaining the geometry, the composite material was assigned. The new weight was equal to 23,91g. It is immediately possible to notice a reduction of about 67% of the weight.

### II. 3. Maximum Compressive Force due to the Gas Pressure

The analysis of the pin was conducted considering the maximum compressive force due to the gas pressure. This force takes into account the gas pressure inside the combustion chamber at each crank degree  $p_g(\theta)$  and the pressure in the crankcase  $p_0$ , equal to the environment pressure if the crankcase compartment would be open.

In the project, the crankcase was considered unsealed with respect to the external environment, so the pressure  $p_0$  was taken equal to 1 atm. The gas pressure values inside the chamber were given by the Politecnico Of Turin. The values are reported in the following plot:

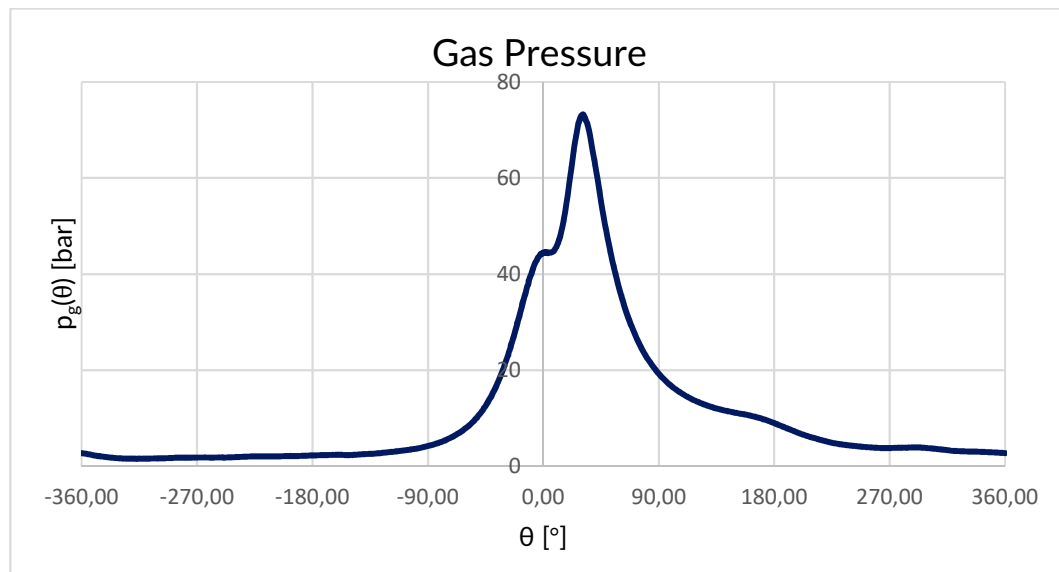


Figure II. 3-1 Gas Pressure Trend

The gas pressure force was evaluated considering that the gas pressure act on the piston surface, so:

$$F_g = [p_g(\theta) - p_0] \frac{\pi D_{piston}^2}{4}$$

Where  $D_{piston}$  is the piston bore and it's equal to 72mm. In this way it was possible to evaluate the force due to the gas pressure at each crank degree.

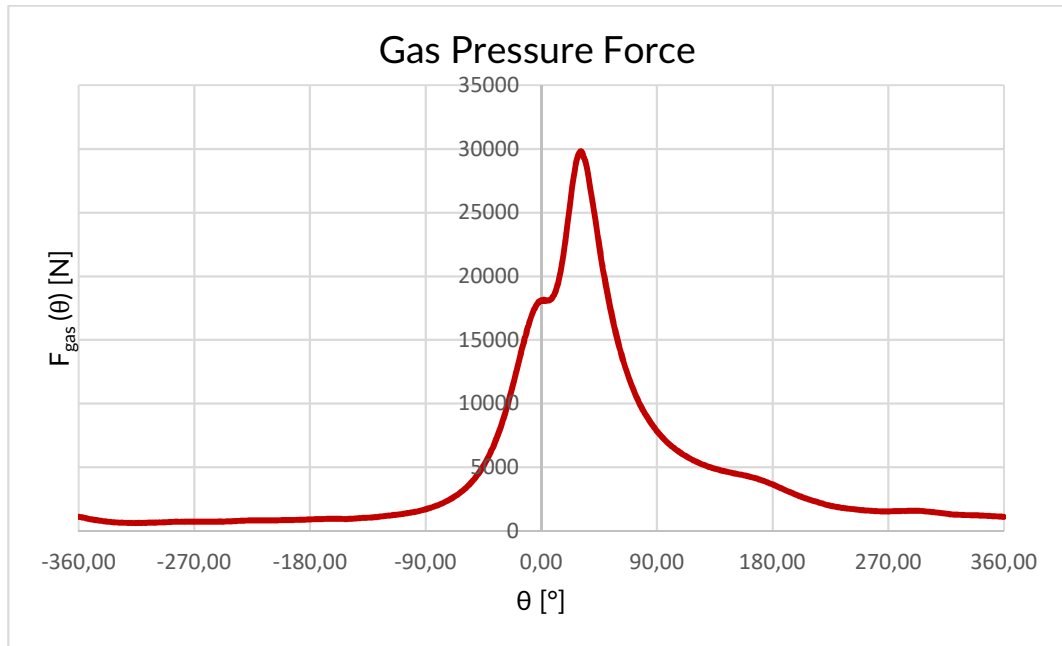


Figure II. 3-2 Gas Pressure Force

From the plot showed in Figure II. 3-2 it is possible to notice that the maximum force due to the gas occurs slightly over the TDC, in particular at  $\theta=31^\circ$ .

### III. Connecting Rod Analysis

As a first analysis, it was considered a standard engine component made of steel. Then the analysis was modified introducing the values for the new material. This caused a change in the values of the masses and so in the inertial forces acting on the engine.

The complex geometry of the connecting rod was reduced to an equivalent simpler one in order to evaluate the forces acting on the component itself. With this procedure it is possible to evaluate individually each component mass. The masses so calculated will be summed up in a proper way to find the total alternating mass.

The alternating mass represents the equivalent mass subjected to the alternating forces. The alternating forces are inertial forces whose direction is aligned with the cylinder axis. These forces vary in value from the Top Dead Center (TDC) to the Bottom Dead Center (BDC) accordingly with the relation showed in the paragraph III.1) 3. .

The starting point for this model was the CAD file given by the Politecnico Of Turin in which the original engine is present. From that file it was possible to take the original geometry and to evaluate the force.

The steps necessary to evaluate the force will be discussed below. It starts with the evaluation of the geometry of the components, followed by the reduction of the geometry into a simpler equivalent geometry, until the final evaluation of the inertial forces.

This procedure is applied to the connecting rod, which represents the connecting element between the different parts interested by the inertial forces. The wrist pin will enter in the calculation in the final evaluation of the alternating mass. The procedure showed below is therefore necessary to evaluate the inertial forces.

#### III. 1. Steel Connecting Rod

##### III.1) 1. Geometrical Parameters

First, it is necessary to know all the geometrical parameters of the engine. Using the CAD file given by the Politecnico Of Turin, it was possible to extract all the values:

<b>Crank Radius</b>	r = 42 mm
<b>Connecting Road Length</b>	l = 128,95 mm
<b>Piston Stroke</b>	L = 84 mm
<b>Piston Bore</b>	B = 72 mm

Table III. 1-1 Geometrical Parameters

From which it was possible to evaluate:

a) Geometrical Ratio  $\lambda$ :

$$\lambda = \frac{r}{l} = \frac{42}{128,95} = 0,325707639$$

Equation III. 1-1 Geometrical Ratio

b) Piston Surface S:

$$S = \pi \frac{B^2}{4} = \pi \frac{72^2}{4} = 4071,504079 \text{ mm}^2$$

Equation III. 1-2 Piston Surface

### III.1) 2. Equivalent Crank Mechanism

Considering the Figure III. 1-1, the next step consisted in reducing the connecting rod to an equivalent one, where the position of the center of gravity (G) and the mass of the connecting rod were taken from the CAD file.

<b>Connecting Rod Mass</b>	$m_{cr} = 428\text{g}$
<b>Small Eye to G Distance</b>	$x_1 = 93,96\text{mm}$
<b>Big Eye to G Distance</b>	$x_2 = 34,99\text{mm}$

Table III. 1-2 Reduced Connecting Rod in Steel

Where:

$$\begin{cases} m_{cr,a} + m_{cr,r} = m_{cr,tot} \\ m_{cr,a}x_1 = m_{cr,r}x_2 \rightarrow \\ m_{cr,a}x_1^2 + m_{cr,r}x_2^2 + J_0 = j_{cr,tot} \end{cases} \begin{cases} m_{cr,a} = m_{cr,tot} - m_{cr,r} = 116,1359\text{g} \\ m_{cr,r} = \frac{x_1}{x_1 + x_2} m_{cr,tot} = 311,8641\text{g} \end{cases}$$

Table III. 1-3 Reduced Conrod Masses (Steel)

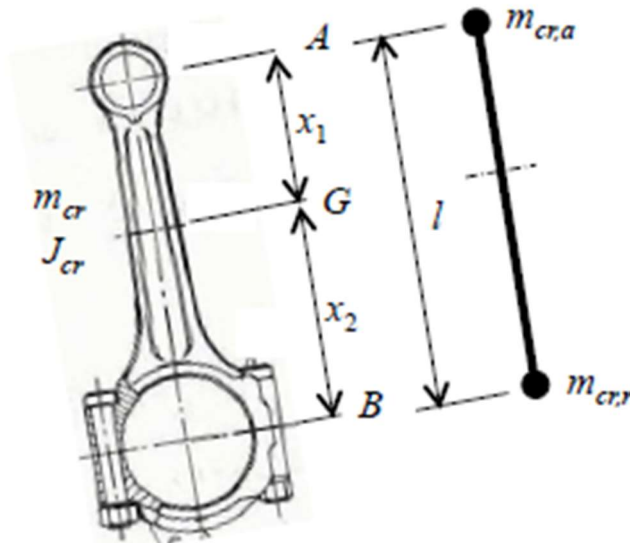


Figure III. 1-1 Reduced Connecting Rod

- $J_0 \approx - (0.01 - 0.03)m_{cr,tot} \frac{r^2}{\lambda^2}$ , is always negative and it has to be added to the moment of inertia of the connecting rod in order to guarantee the conservation of the total moment of inertia.

### III.1) 3. Evaluation of the Alternating Forces

In order to evaluate the alternating forces, it was necessary to calculate the value of the alternating mass  $m_a$ :

$$m_a = m_p + m_{wp} + m_{cr,a} = 218g + 72g + 116,14g = 406,14g$$

Equation III. 1-3 Alternating Mass for Steel Conrod

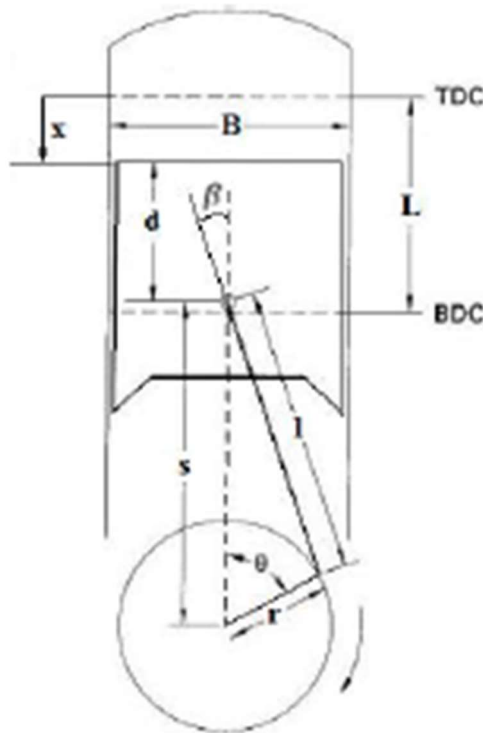


Figure III. 1-2 Centered Crank Mechanism Layout

Where  $m_p$  is the piston mass (including elastic rings),  $m_{wp}$  is the wrist pin mass and  $m_{cr,a}$  is the mass evaluated previously.

Referring to the centered crank mechanism layout in Figure III. 1-2 the reciprocating parts that move along the cylinder axis are then subjected to the inertial force:

$$F_a = -m_a a_p = -m_a \omega^2 (\cos \vartheta + \lambda \cos 2\vartheta)$$

Equation III. 1-4 Alternating Inertial Force

- $\omega$  is the maximum rotational speed of the engine expressed in radiant per second:

$$\omega = n \frac{2\pi}{60} = 6250 \frac{\pi}{30} = 654,5 \text{ rad/s}$$

Equation III. 1-5 Maximum Rotational Speed

- $\theta$  is the rotation angle of the crank with respect to the Top Dead Center (TDC)

As it is possible to notice, this force is proportional to the square of the rotational speed of the crankshaft. So, even a small increment in the rotational speed of the engine brings to a remarkable increment of the inertial force.

### III.1) 4. Evaluation of the Centrifugal Force

In order to show properly the effects of the composite material components inside the engine, a further inertial force must be introduced. In the paragraph “Evaluation of the Alternating Forces” only the reciprocating force was analyzed. To evaluate the forces on the engine block, all the forces must be considered.

The centrifugal force acting on the rotating parts of the engine can be evaluated as follow:

$$F_{\omega} = m_r \omega^2 r$$

Equation III. 1-6 Centrifugal Force

The centrifugal force is a rotating vector with constant amplitude which pass through the axis of rotation of the crank.

The relation Equation III. 1-6 considers all the bodies  $m_r$  involved in the rotating motion reduced at the crank radius  $r$ . The term  $m_r$  has to be evaluated considering all the rotating parts involved: the connecting rods  $m_{cr,r}$ , the crank webs  $m_{cw}$  and the crank pins  $m_{cp}$ :

$$m_r = m_{cp} + 2m_{cw,red} + m_{cr,r}$$

Equation III. 1-7 Rotating Mass

The crank web mass  $m_{cw}$  is generally placed at a certain distance  $r_{cw}$  from the crank axis. It is necessary to reduce that mass to the crank radius. To do so, based on the Figure III. 1-3, the equality of static moments was imposed:

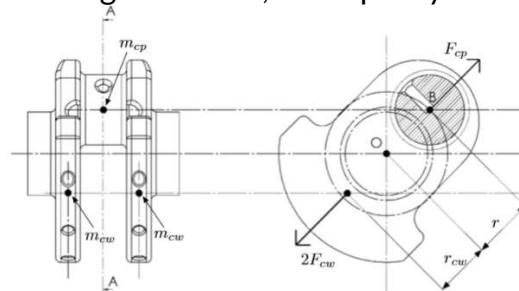


Figure III. 1-3 Crank mass reduction

$$m_{cw,red} = m_{cw} \frac{r_{cw}}{r}$$

Equation III. 1-8 Reduced Crank Web Mass

For the steel components, the values of the centrifugal force and the relative masses are shown in the following:

$$m_r = m_{cp} + 2m_{cw,red} + m_{cr,r} = 233,61g + 2(120,42g) + 311,86g = 786,32g$$

Equation III. 1-9 Rotating Mass for Steel Components

$$F_{\omega} = m_r \omega^2 r = \frac{786,32}{1000} kg \left( \frac{654 rad}{s} \right)^2 0,042m = 14147,04 N$$

Equation III. 1-10 Centrifugal Force for Steel Components

The value of the centrifugal force is referred to the maximum rotating speed of 6250 rpm.

### III. 2. Composite Connecting Rod

Once the model was defined, it was possible to modify the values of the masses for the composite components. The geometry is still the same. The values for the masses was found through Solidworks assigning the composite material to the CAD geometry.

In this way it was possible to see that the masses were almost the half of the original component mass. The masses are showed in table below, in which the original masses are present to compare the values:

<b>Composite Con. Rod</b>	$m_{cr, comp} = 201,98g$	<b>Steel Con. Rod</b>	$m_{cr, steel} = 428g$
<b>Composite Wrist Pin</b>	$m_{wp, comp} = 23,91g$	<b>Steel Wrist Pin</b>	$m_{wp, steel} = 72g$

Table III. 2-1 Mass Comparison

Consequently, also the position of the center of gravity and of the other masses changed. Table below shows the updated values:

<b>Small Eye - Center of Gravity Distance</b>	$x_1 = 96,08mm$
<b>Big Eye - Center of Gravity Distance</b>	$x_2 = 33,29mm$
<b>Small Eye Mass</b>	$m_{cr,a} = m_{cr,tot} - m_{cr,r} = 51,97g$
<b>Big Eye Mass</b>	$m_{cr,r} = \frac{x_1}{x_1 + x_2} m_{cr,tot} = 150,01g$

Table III. 2-2 Big Eye and Small Eye

#### III.2) 1. Alternating Mass for Composite Material

Finally, the alternating mass changed:

$$m_a = m_p + m_{wp} + m_{cr,a} = 218g + 23,91g + 51,97g = 293,88g$$

Equation III. 2-1 Composite Alternating Mass

Notice that the alternating mass evaluated using the composite material is almost the half of the steel alternating mass, just by reducing two components masses. This stresses once again the importance of this kind of materials.

#### III.2) 2. Centrifugal Force for Composite Material

<b>Rotating Mass</b>	<b>Centrifugal Force</b>	<b>Reduction</b>
$m_r = 624,46 g$	$F_\omega = 11234,97 N$	20,48 %

Table III. 2-3 Rotating Mass and Force for Composite Components

The value of the centrifugal force is referred to the maximum rotating speed of 6250 rpm.

### III. 3. Results and Comparison between Steel and Composite

Once the model was designed, some hypothesis should be done. First, the rotational speed imposed was the maximum available for the engine, so 6250 rpm. Therefore, the results of the calculation refer to the worst possible case.

Second, in the results showed in Figure III. 3-1 it must be considered that the x-axis is downward. This means that in traction phase, the force values are negative since their direction is opposed to x-axis (referred to Figure III. 1-2); vice versa in compression phase.

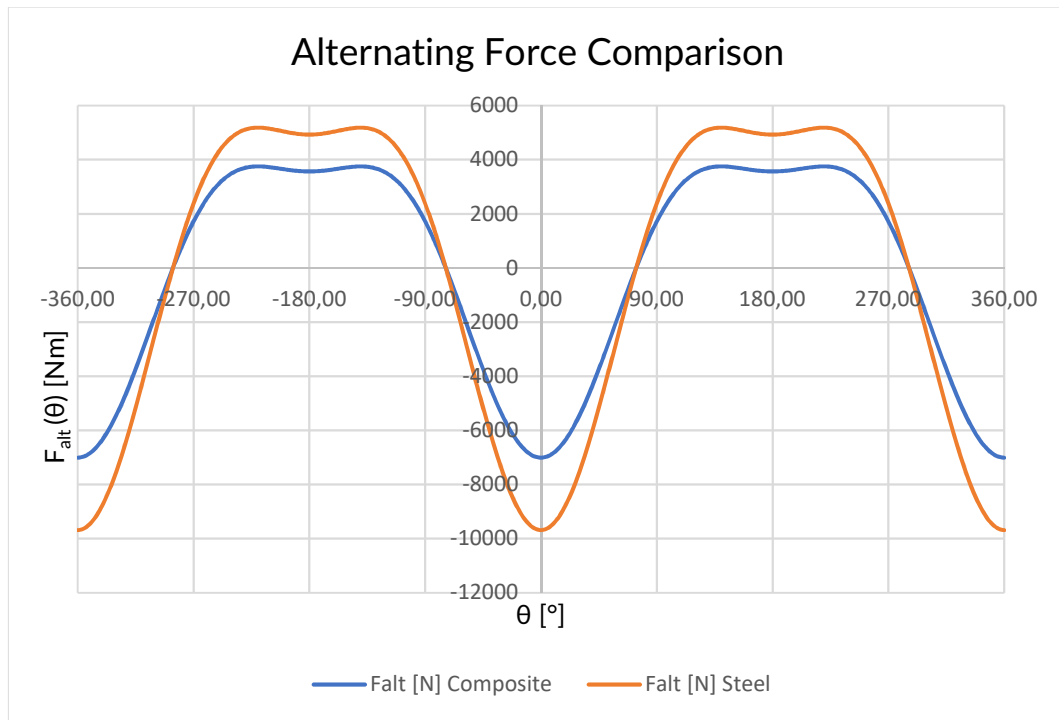


Figure III. 3-1 Alternating Forces Comparison

It is possible to notice that the curve for the composite material always lays below the curve for steel components. Once again, the substitution of two steel components of the engine with composite ones had a highly beneficial effect on the engine.

Maximum compression forces are:

Steel Components	Composite Components
$F_{\max\text{Compr\_Steel}} = 5184,19 \text{ N}$	$F_{\max\text{Compr\_Composite}} = 3751,34 \text{ N}$

Table III. 3-1 Maximum Compression Force Comparison

Minimum alternating forces, so maximum traction forces are:

Steel Components	Composite Components
$F_{\max\text{Tract\_Steel}} = -9686,92 \text{ N}$	$F_{\max\text{Tract\_Composite}} = -7009,56 \text{ N}$

Table III. 3-2 Maximum Traction Force Comparison

Note that the maximum value of the alternating force reduced from 9686,92 N for the steel components to 7009,56 N for the composite components, a reduction of about the 28%.

The equation for the torque available at the crankshaft is equal to:

$$T = Fr(\sin\theta + \frac{\lambda}{2}\sin 2\theta)$$

Equation III. 3-1 Cylinder Block Torque

Where  $F$  is the resultant force acting on the crank mechanism, equal to the sum of the force due to the gas pressure  $F_g$  and the alternating force  $F_a$ :

$$\begin{cases} F = F_g + F_a \\ F_g = [p_g(\theta) - p_0] \frac{\pi D^2}{4} \\ F_a = -m_a \omega^2 (\cos(\vartheta) + \lambda \cos 2\vartheta) \end{cases}$$

Equation III. 3-2 Resultant Force on Crank Mechanism

The torque comparison is showed in the following plot:

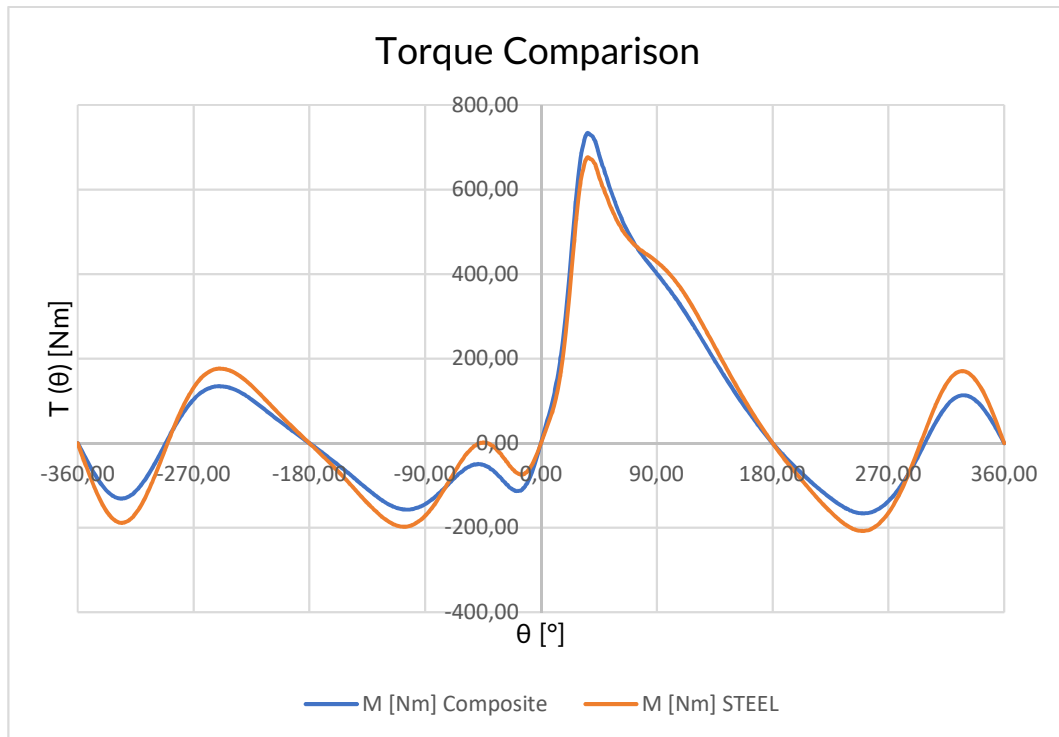


Figure III. 3-2 Torque Comparison at the crankshaft

The value of force used in the simulations is the total force  $F$  between the alternating force and the gas pressure force:

$$F_{Tot} = F_g + F_a$$

Equation III. 3-3 Total Force acting on the Pin

This force was evaluated at different crank angles  $\theta$ , and its trend is:

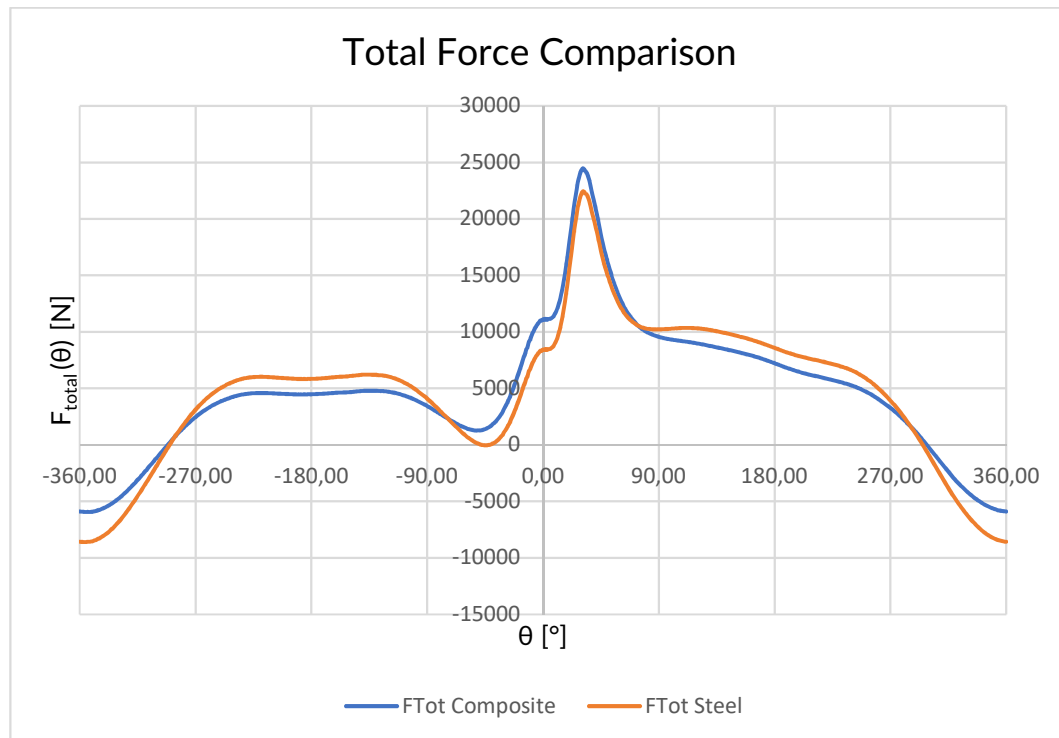


Figure III. 3-3 Total Force Comparison between Steel and Composite

From Figure III. 3-3 it is possible to notice that the maximum force occurs slightly over the TDC, in particular at  $\theta=31^\circ$ . For values of  $\theta$  around the TDC ( $0^\circ < \theta < 90^\circ$ ), the total force in composite case is higher than the one for the steel case. This is due to the beneficial effect of the reduction in the inertial forces. This phenomenon can be explained taking into account that the gas pressure at TDC push down the piston, and so the wrist pin, while the inertial force tend to pull up the connecting rod, and again the pin. Around the Top Dead Center the gas pressure force tends to be reduced by the alternating force causing a lower available torque at the crankshaft.

After the TDC, the gas pressure tends to lose its prevailing effect and the inertial force will be the main resistance against the spinning of the crankshaft. In this case the steel case curve will be higher than the composite one. This means that during the rotation of the crank, the “inertial resistance” of the composite components will be lower than the resistance offered by the steel components.

In both cases it's possible to notice the beneficial effects due to the introduction of composite material components inside the engine.

## IV. Analysis Method

The main problem with this software was the not complete implementation of the composite material for solid layered elements. Actually, the software doesn't allow to manage easily the material orientation. Even the special tool dedicated to the orientation review doesn't show the direction of the fibers. For this reason, many trials were performed to find the correct solution for the problem.

The force involved in the simulation was the total force, sum of the gas pressure force and the alternating force. In particular, the force value is equal to  $F_{Tot} = 24473,3 \text{ N}$  and its direction is vertical (y-axis). It can be considered as an approximation since this value of the force, the maximum one, is reached slightly over the Top Dead Center, so it would be inclined with respect to the vertical. Even with this approximation, the wrist pin model will be correct. Indeed, the two geometry models involved in the simulations are both axially symmetric. In this way it was possible to consider the force always vertical with respect to the wrist pin axis.

### IV. 1. Geometry Models

Two geometry models were developed:

- 1- **Alone Pin Model (APM)**: the initial analysis was conducted on the pin only to simplify the calculations. Since its aim was to study the case as a first attempt, only the laminate tool model will be discussed as APM;

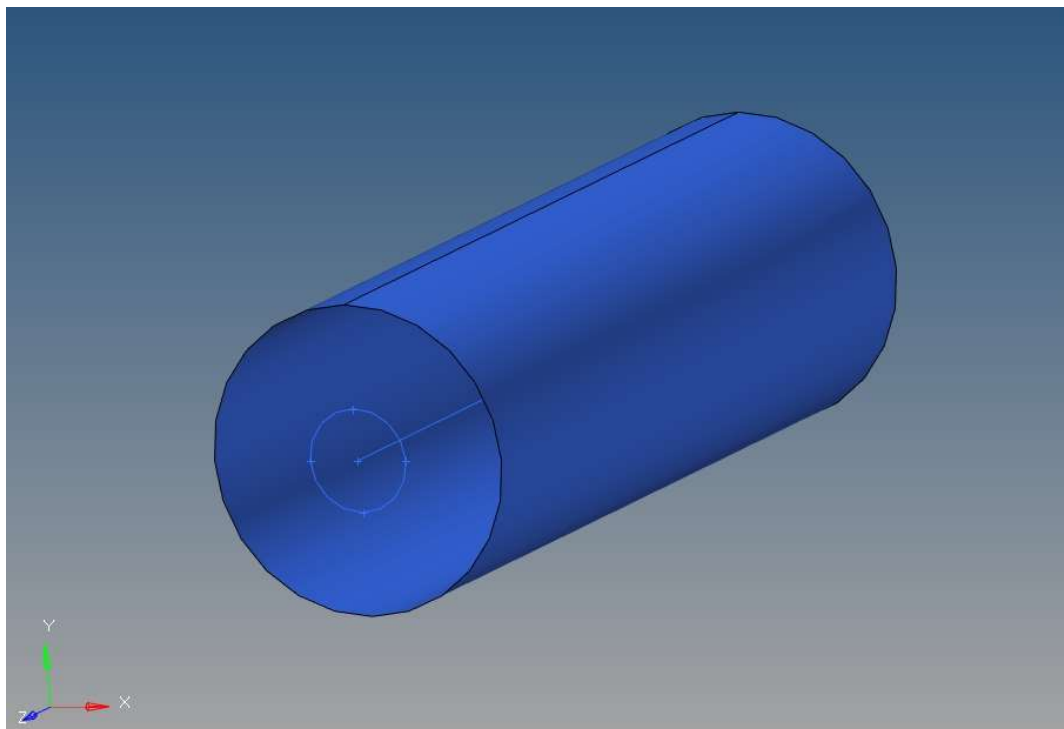


Figure IV. 1-1 APM Model

- 2- **Semi-Complete Pin Model (SCPM)**: the APM wasn't representative of the actual case. Consequently, the model was updated with two supports

(equivalent to the piston hubs) and part of the connecting rod. Including the complete models of the piston and of the connecting rod would have brought to an excessive complexity of the model. So, the choice was to reduce the system composed by the piston, the wrist pin and the connecting rod to an equivalent one, showed in Figure IV. 1-2 SCPM Model:

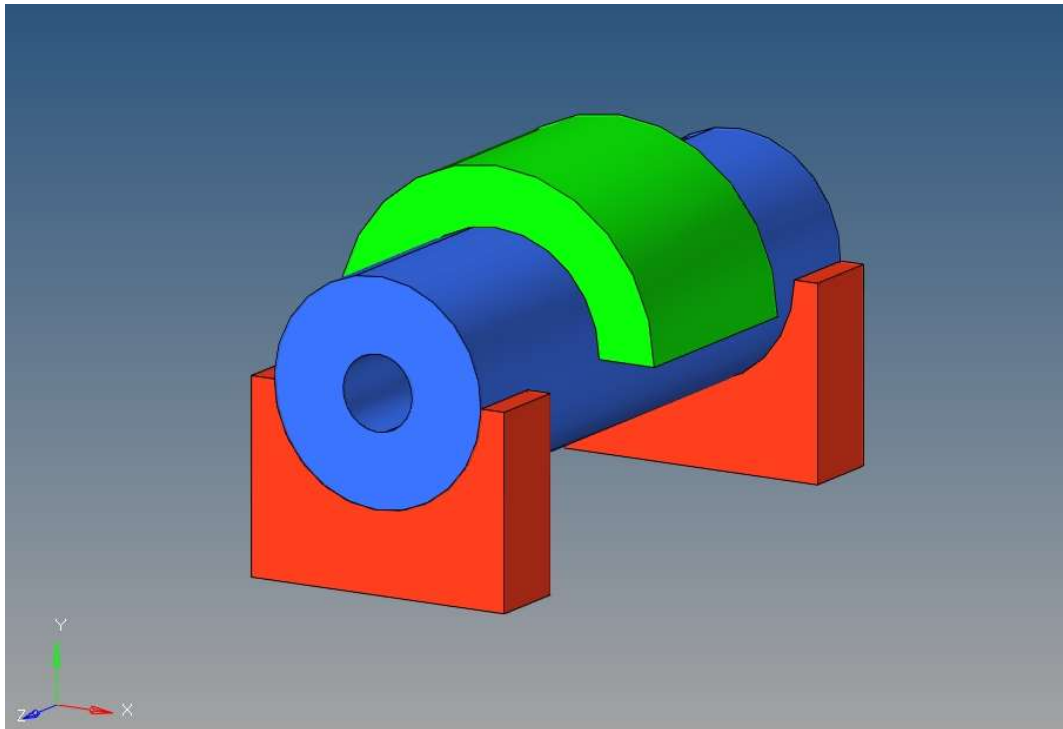


Figure IV. 1-2 SCPM Model

This model was used for the Solid Layer Shell, that will be discussed later. In the Paragraph IV.2) 2. *Altair Hypermesh – Layered Solid Shell using PCOMPLS*, since the focus of the project is the wrist pin, only the pin will be modeled with PCOMPLS elements. Supports and connecting rod will be modeled as PSOLID elements.

## IV. 2. *Altair Hypermesh*

### IV.2) 1. *Altair Hypermesh – Layered Shell using Laminate Tool*

First step was to create the Material Card with all the material characteristics. To create a Laminate, a particular property called PCOMPP was created. Inside this card it was possible to define two main parameters for the laminate: the allowable interlaminar shear stress, set to 70 MPa (typical value for epoxy matrix), and the failure theory, set as *TSAI*, to obtain the Tsai-Wu Failure Index as output result. These parameters were necessary to evaluate properly the failure index of the laminated component.

Name	Value
Solver Keyword	PCOMPP
Name	PCOMPP
ID	4
Color	
Include	[Master Model]
Defined	<input checked="" type="checkbox"/>
Card Image	PCOMPP
User Comments	Hide In Menu/Export
<input type="checkbox"/> Z0 OPTIONS	REAL
Z0	0.0
NSM	
SB	70.0
FT	TSAI

Figure IV. 2-1 PCOMPP Property Card

To create a laminated component, it was possible to use a specific tool available in the *Properties* panel.

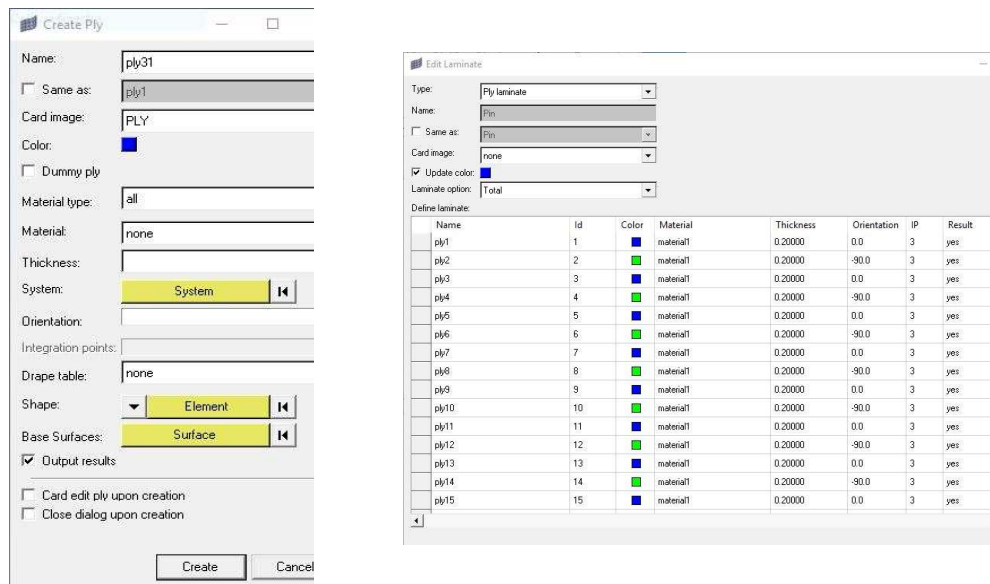


Figure IV. 2-2 Laminate Tool

The *Ply Tool* allows to create different plies. Material, thickness and orientation can be chosen for each ply. Thirty plies were created, fifteen with longitudinal direction and fifteen with circumferential direction. The two directions were chosen to react to shear stresses, and consequently to bending. Longitudinal fibers will react to bending, circumferential will react to shear.

The choice of thirty plies was done because carbon fibers plies in actual components are usually 0.2mm thick. Considering that the pin thickness is equal to 6mm, thirty plies represent the correct plies number. This choice will be valid also for the next solid layer model.

Name	Value
Solver Keyword	MAT8*
Name	UD-Material (PEI-AS4)
ID	1
Color	
Include	[Master Model]
Defined	<input checked="" type="checkbox"/>
Card Image	MAT8
User Comments	Hide In Menu/Export
E1	128700.0
E2	7600.0
NU12	0.28
G12	4800.0
G1Z	
G2Z	
RHO	1.51e-009

Figure IV. 2-3 MAT8 Material Card

The material card was chosen as *MAT8*. The correct card would be *MAT9ORT*, but the laminate tool isn't compatible with it. *MAT8* card is compatible with the laminate tool and defines the material properties for linear temperature-independent orthotropic material for two-dimensional elements.

After the creation of the plies, the laminate can be created. To create the laminate, the Laminate Tool was used (Figure IV. 2-2). This tool allows to stack the different plies. The result is showed in Figure IV. 2-4:

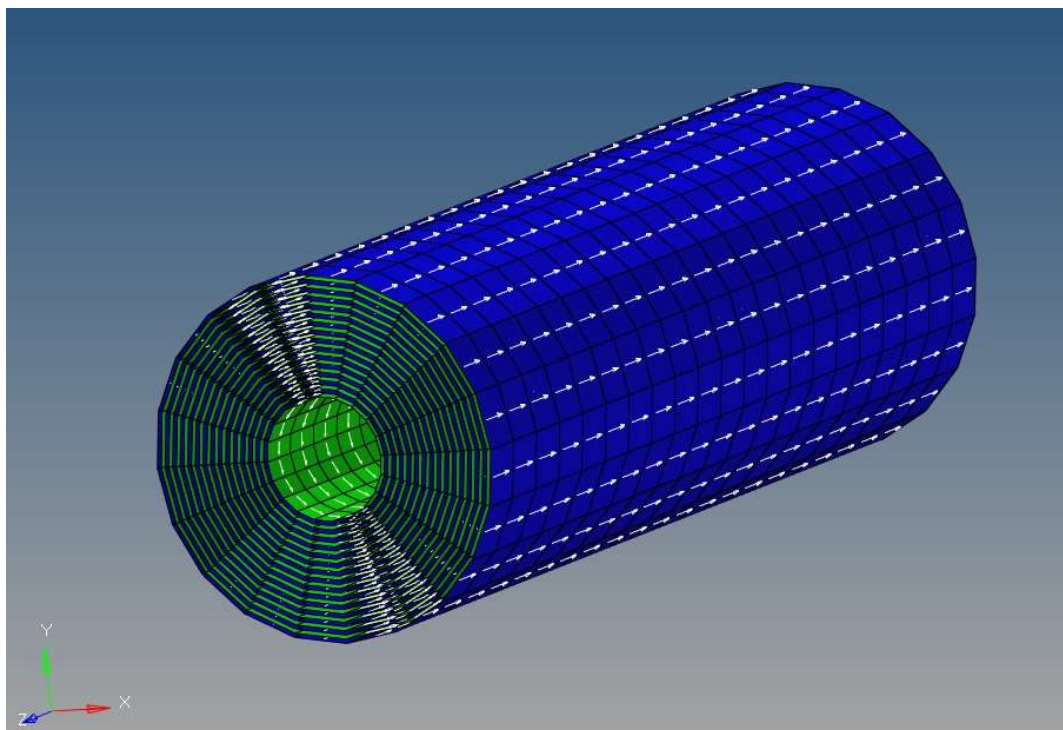


Figure IV. 2-4 Laminate Model

Once the geometry and the stratification were completed, loads and constraints were defined as shown in Figure IV. 2-5.

To apply the vertical force (yellow arrow in the Figure IV. 2-5) a rigid element RBE3 was created. The rigid RBE3 creates a “spider” element which doesn’t introduce any additional stiffness to the component. The independent node displacement is an average weight of the dependent node displacements. This rigid element was created to simulate the connecting rod over which the load would apply. Only for this simple case, the force value was taken equal to the maximum alternating force in case of traction, so  $F_{alt} = 7009,6 N$ .

The constraints indicated by the red triangles in Figure IV. 2-5, were applied to a part of the circumference of the pin. The hypothesis behind this configuration is that the pin is supported by the piston hubs only in a certain portion. The numbers over the constraints represent the degrees of freedom of the constraints. The numbers “123” indicate that the pin is constrained in the three translation directions x,y and z, but it can rotate in the three directions.

This configuration represents a huge limit to the “reality” of the model for two main reasons: the introduction of a rigid element directly connected to the pin could modify the result of the analysis; the constraints so positioned are not well representative of the actual piston hubs. They increase the stiffness of the pin, bringing to an overestimated resistance of the component. The analysis was set as linear static. It is not representative of the actual case but can be initially accepted as first attempt.

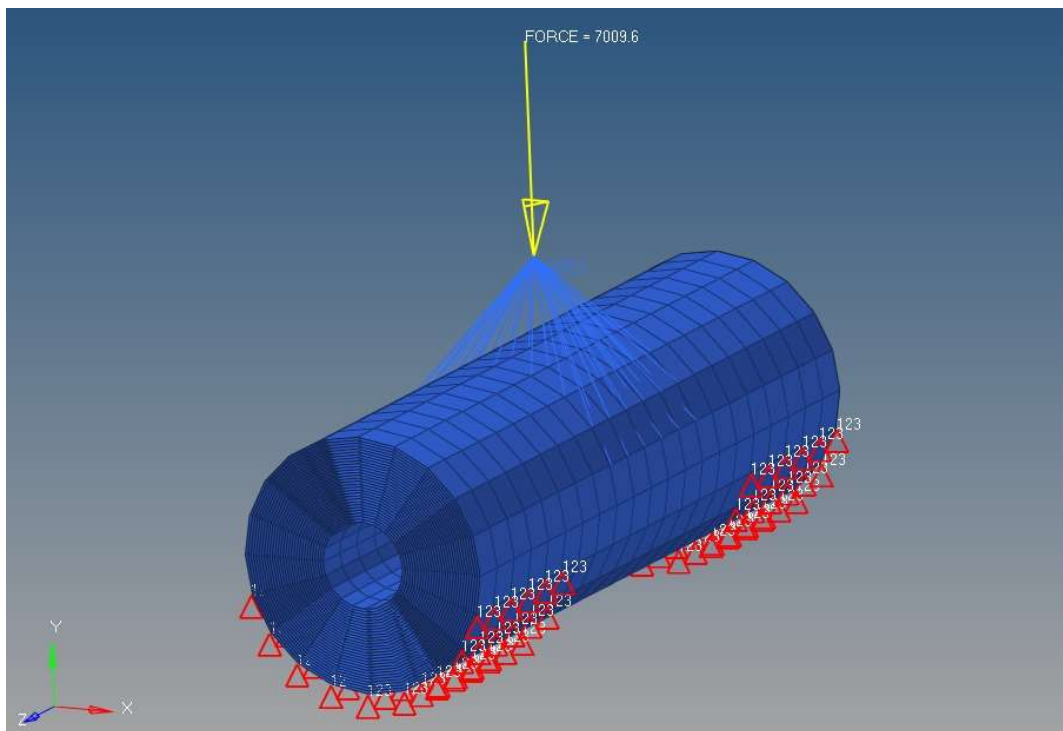


Figure IV. 2-5 Laminate Model with loads

Through this method it was possible to create a first setup for the model. Since this model represents the first attempt for the analysis, APM model was used. The Laminate Tool allows to create “SHELL” elements, that are surface elements. These elements are good if a certain dimension hypothesis is valid: the main length should be at least 10-15 times with respect to the lower dimension. In the wrist pin case, the length of the pin is 52.5 mm, while its

thickness is 6 mm. Then the use of the surface element would bring us to an unsolicited approximation. Still, the results showed in Figure IV. 2-6 are a good start point for the next phases.

This limit is well exposed in the result of HyperView, the post-processor software of Altair. As it is possible to see in Figure IV. 2-6, the component is treated as a shell, with a negligible thickness.

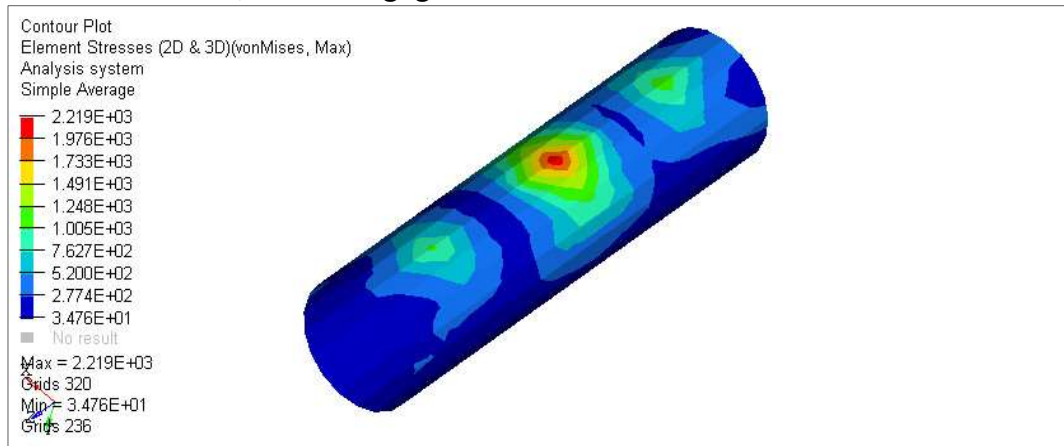


Figure IV. 2-6 Laminate Model Results

Afterwards, a SCPM was created also for the Laminate Tool (Figure IV. 2-7). The reason for this choice was to generate a model to be compared to the results of the solid layered elements. The model includes a laminated pin with thirty plies, oriented at 0° and 90°, two supports and a reduced connecting rod.

The differences with the first model are:

- Constraints on the supports, blocked in all their degrees of freedom and on the conrod faces, to constraint the connecting rod and allow the convergence of the simulation;
- Force applied on a RBE3 rigid element and equal in value to the maximum total force (gas pressure plus alternating force), so  $F_{Tot}=24473,3\text{ N}$ ;
- Contacts between the surfaces;

More details about these differences in terms of realization and meaning can be found in the next paragraphs.

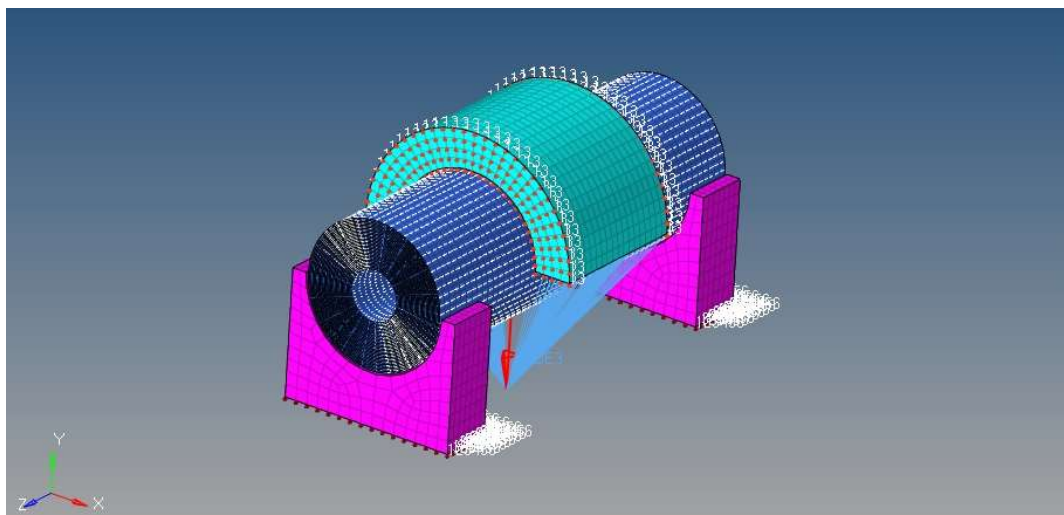


Figure IV. 2-7 Complete Laminated Component Model

**IV.2) 2. Altair Hypermesh – Layered Solid Shell using PCOMPLS**

In order to increase the precision of the results, a new model was developed. In this case the layers were realized through a property called PCOMPLS. This property defines global ply-based composite properties for layered solid shell composites. Regarding the elements, type of analysis and material, PCOMPLS is only supported for CHEXA and CPENTA elements (solid mesh elements). Also, it is compatible with linear and nonlinear analysis (small and large displacement) and MAT1, MAT9 and MAT9ORT material types.

Name	Value
Solver Keyword	MAT9ORT
Name	UD-Balanced Pin
ID	1
Color	
Include	[Master Model]
Defined	<input checked="" type="checkbox"/>
Card Image	MAT9ORT
User Comments	Do Not Export
E1	128700.0
E2	7600.0
E3	7600.0
NU12	0.28
NU23	0.28
NU31	
RHO	1.55e-009
G12	4800.0
G23	4800.0
G31	2968.75

Figure IV. 2-8 MAT9ORT Material card

MAT9ORT card was chosen for this part of the project. This card defines the material properties for linear, temperature-independent, and orthotropic materials for solid elements. The biggest difference from MAT8 is that MAT9ORT can be used as material card for solid elements.

Referred to the Altair Connect page, PCOMPLS format is showed below:

(1)	(2)	(3)	(4)	(5)
PCOMPLS	PID		CORDM	
	IDi	MIDi	Ti	THETAi

Table IV. 2-1 PCOMPLS Format

PID	Unique composite property identification number
CORDM	Identification number of the material coordinate system

IDi	Global Ply ID. Ply numbering follows this thickness direction
MIDi	Material ID for the ply defined via the previous IDi field
Ti	<p>Defines the actual thickness of the ply specified via the IDi field</p> <p>The actual ply thicknesses depend on the actual total geometric thickness of the solid element. The calculation is as follows:</p> $T_{actual}^{ply_i} = T_{actual}^e \left( \frac{T_i}{T_1 + T_2 + \dots + T_N} \right)$ <p style="text-align: center;"><i>Equation IV. 2-1 Ply Thickness Evaluation</i></p> <p>Where:</p> <p><math>T_{actual}^{ply_i}</math> is the actual thickness of the ply “i”;</p> <p><math>T_{actual}^e</math> is the actual (or geometric) thickness of the composite element;</p> <p><math>T_i</math> are the user-defined ply thickness via the Ti fields on the PCOMPLS entry.</p>
THETAi	<p>Orientation angle of the ply within the ply plane*. The X-axis coordinate system defined via CORDM (basic system, if blank) is projected onto the ply plane. The orientation angle is measured from this projected X-axis along the projected Z-axis.</p> <p>The ply plane is defined perpendicular to the thickness direction of the composite element. The thickness direction by default starts from face G1-G2-G3-G4 to face G5-G6-G7-G8 of the solid element.</p> <p>The orientation angle is measured positive counterclockwise direction from the projected X-axis about the local Z-axis of the ply.</p> <div style="text-align: center;"> <p style="text-align: center;"><i>Figure IV. 2-9 PCOMPLS Reference System</i></p> </div>

Table IV. 2-2 PCOMPLS Details

The potential of this kind of elements is very high, but the software is not optimized in their use. Aim of this project was also to deepen the use of PCOMPLS.

PCOMPLS allows to create a unique mesh of the object and to define, inside the volumetric mesh, different numbers of plies. In particular, it was possible to define number and thickness of each ply. With the version of the software HyperMesh 2017.3 it wasn't possible to modify the THETA boxes.

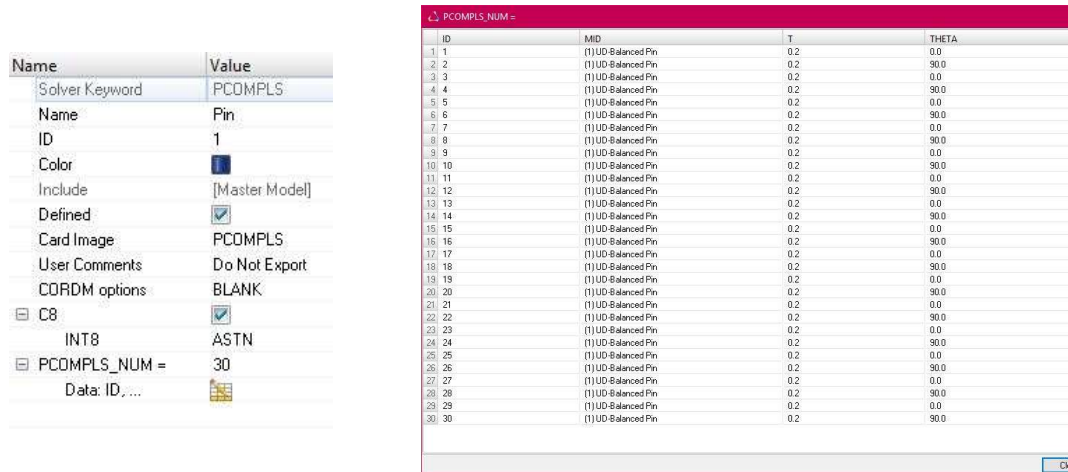


Figure IV. 2-10 PCOMPLS Property Card

Particular attention must be put to the *THETA* boxes. As told before, the software is still developing the PCOMPLS elements and their functionality. In order to solve this problem a particular procedure must be followed. It is necessary to complete the entire model and run it on the solver Optistruct or extract it as *.fem* file. The *.fem* file contains all the information about the model, such as material, nodes, properties, forces and constraints. It is necessary to open the *.fem* file with a text editor, like notepad. Scroll to the properties and modify manually the column corresponding to theta in PCOMPLS:

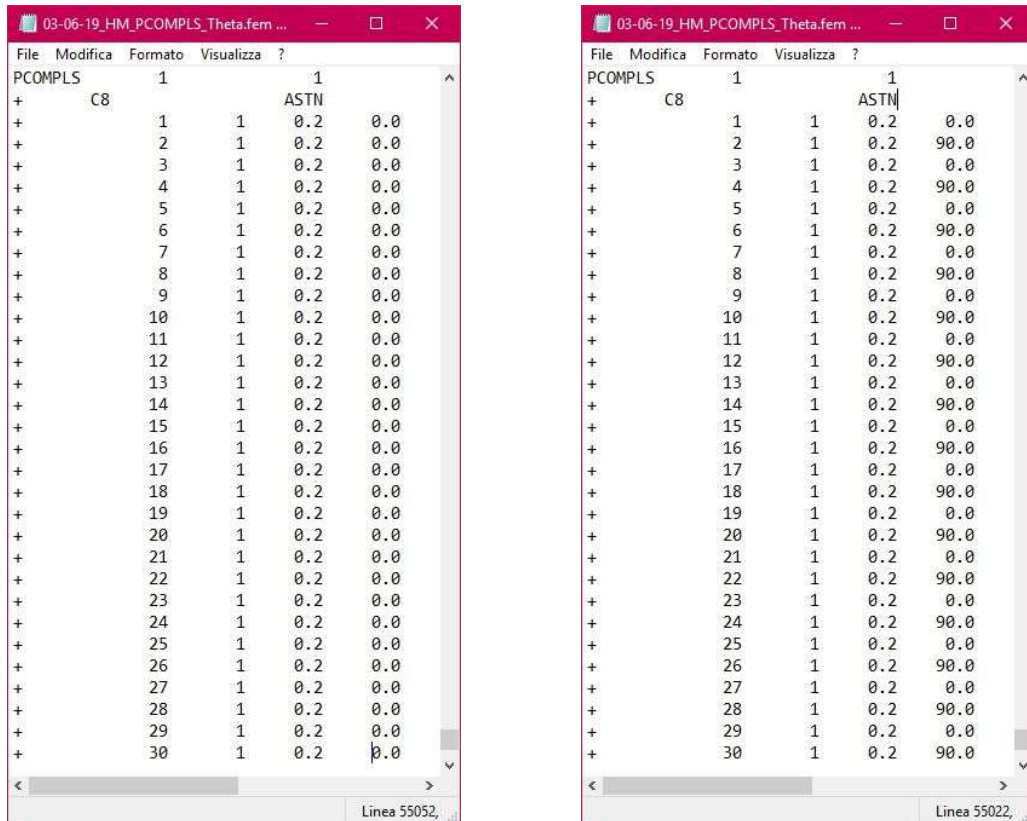


Figure IV. 2-11 Manual variation of the THETA by using .fem file

To obtain a correct orientation of the fibers along the component a coherent reference system was developed. It consists of a Cartesian reference system centered at the center of the pin oriented in a such way that the local x-axis of the system is aligned with the length of the pin, as showed in the Figure IV. 2-12:

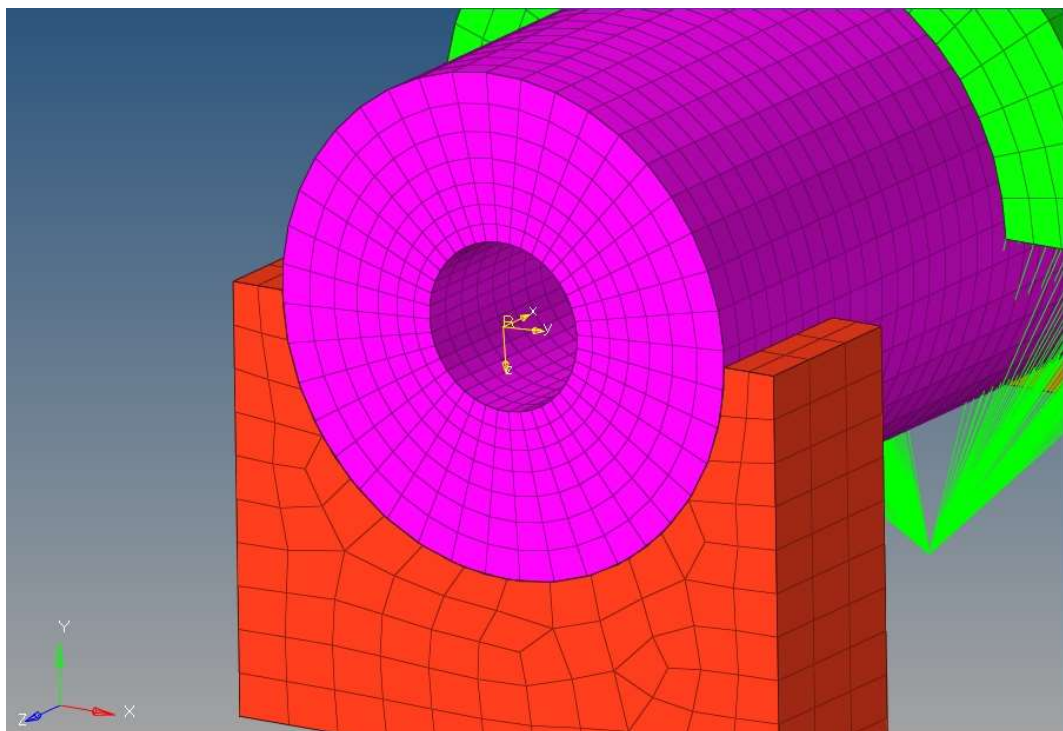


Figure IV. 2-12 PCOMPLS Reference system in the model

As it is possible to notice in Figure IV. 2-12, the mesh on the pin is unique and continuous, without the need to create each layer separately. This would bring to a great time reduction in the meshing process.

Nest step consisted in putting correctly the boundary conditions. The laminate tool analysis was performed as *linear static* since no contacts, so any non-linearity source, between parts were introduced. This time the presence in the model of different components, such as the reduced connecting rod and the supports, introduced a constraint in the model. Indeed, these parts must be connected to each other by a contact surface.

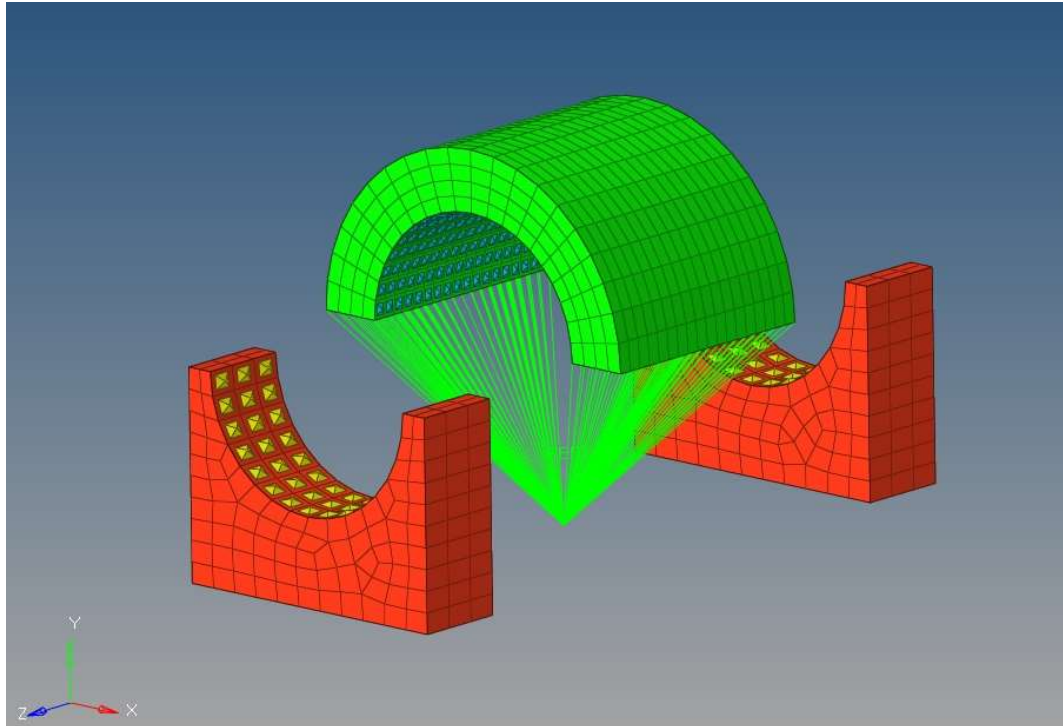


Figure IV. 2-13 Contact surfaces

The contacts card was chosen as *PCONT* and two types were created: “*FREEZE*” contact was used to group together the pin and the supports (yellow boxes in Figure IV. 2-13). This kind of contact simulate a rigid contact between the selected surfaces, which is representative of the actual condition. Indeed, the pin and the piston are rigidly connected through a bushing; “*SLIDE*” contact was used to group together the pin and the conrod (azure boxes in Figure IV. 2-14). This kind of contact simulate a sliding contact between the selected surfaces, as the pin slides inside the conrod.

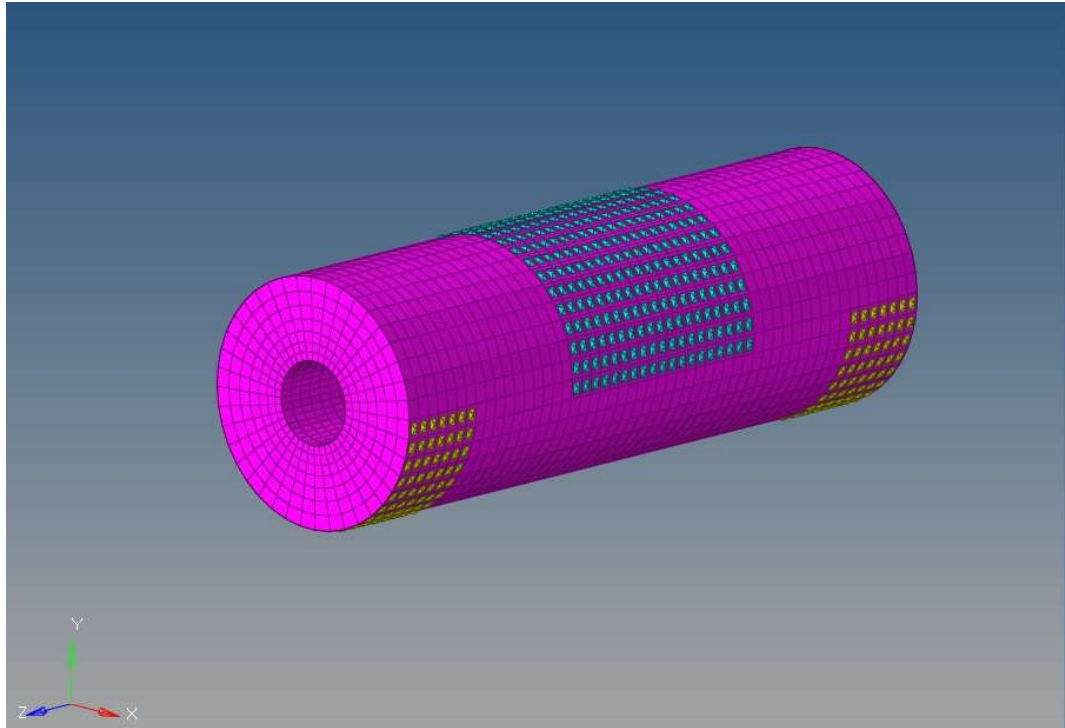


Figure IV. 2-14 Contact groups

The presence of the contacts introduced a strong non-linearity of the model and it increased notably the computational time. Also, the *SLIDE* contact must be properly constrained. For this reason, some constraints were put in order to complete the simulation.

The contact between parts is treated from the software in a particular way. First the parts are considered separated. At the beginning of the simulation the solver moves the parts until they enter in contact. Once the contact occurs, the deformation of the parts starts and the simulation goes on until convergence is reached.

About supports constraints, the Figure IV. 2-15 shows the layout of them:

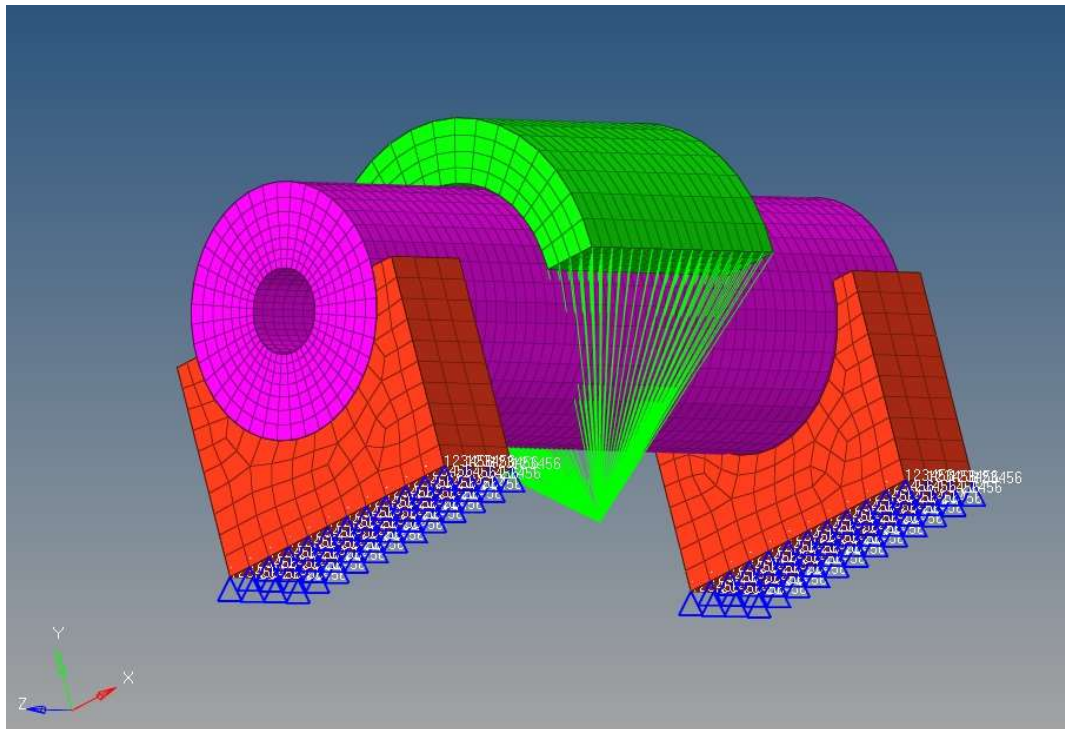


Figure IV. 2-15 PCOMPLS Supports Constraints

The supports constraints were chosen in order to block all the degrees of freedom, so they represent the fixed parts. They can't translate or rotate in any direction.

As said before, the sliding contact between the connecting rod and the wrist pin was a source of divergence. To solve this problem the reduced connecting rod was initially supported with "cart supports" along its surface, as shown in Figure IV. 2-16. The connecting rod was constrained in a such way that it could translate only vertically along Y-axis. This ploy was fundamental in order to make the simulation run to a convergent solution. Without these constraints the connecting rod would rotate around its position and make the simulation diverge.

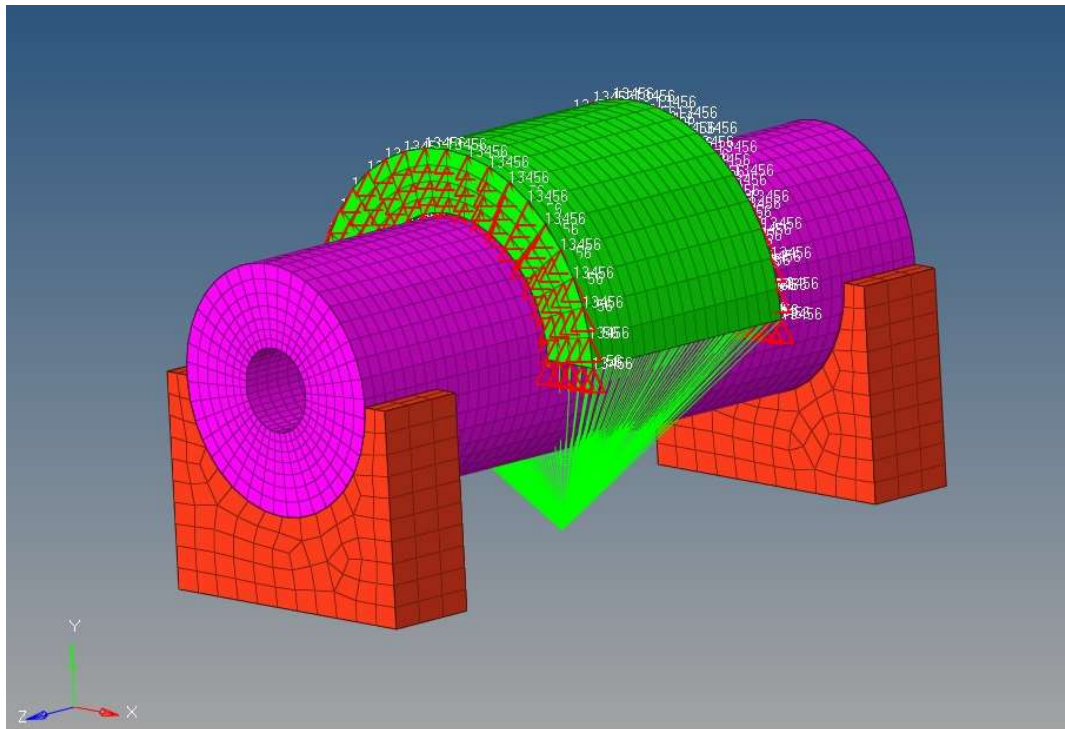


Figure IV. 2-16 Supports on the reduced connecting rod

Subsequently this choice was changed in order to reduce as much as possible the variation of the component stiffness. The introduction of the supports modifies the stiffness of the connecting rod in a non-realistic way, so the supports were removed from the conrod faces and put on a rigid element RBE2. This rigid allows not only to support the connecting rod, but also to load the component with the traction force, as shown in Figure IV. 2-17 and Figure IV. 2-18.

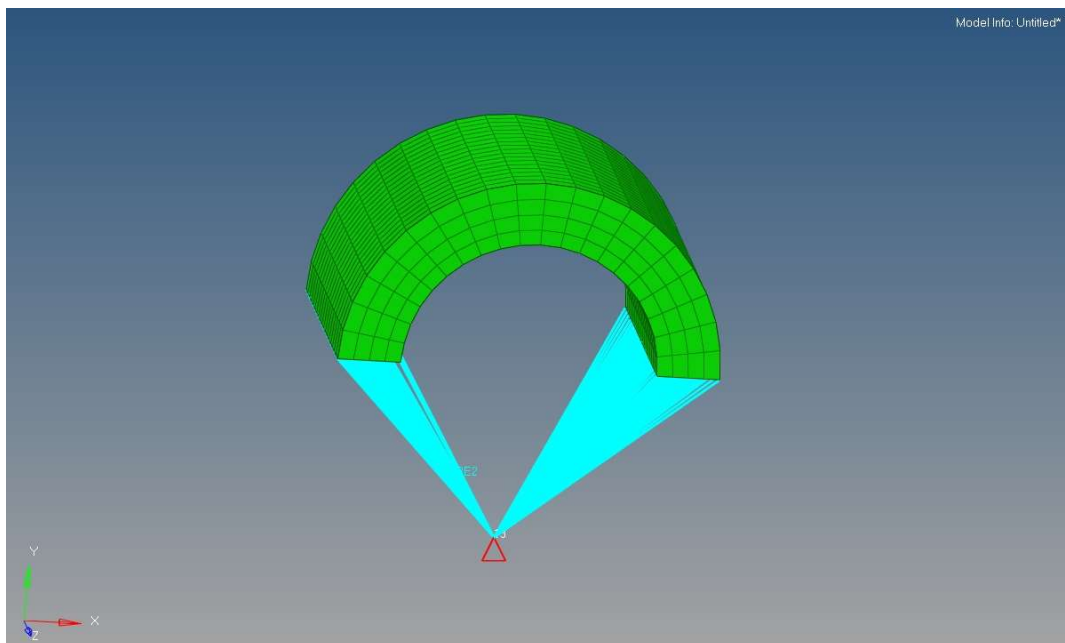


Figure IV. 2-17 Constraint on RBE2 element

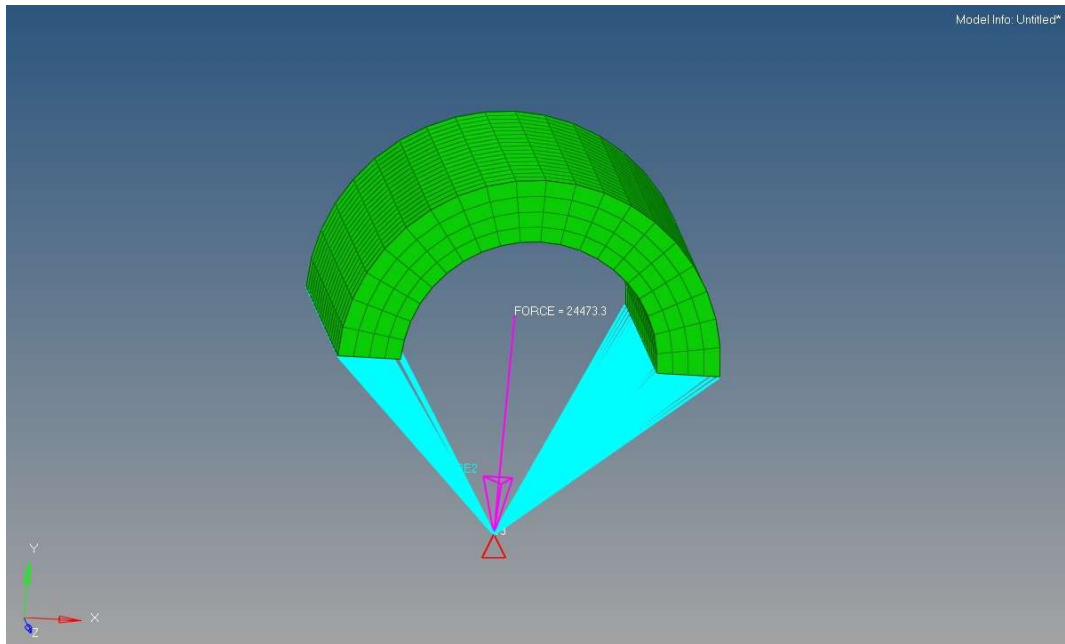


Figure IV. 2-18 Force and Support on RBE2

In this way it was possible to reduce the influence of the rigid on the pin. As seen in *Altair Hypermesh - Layered Shell using Laminate Tool* paragraph, the force should be applied on a RBE3 element. Since it was necessary to anchor the connecting rod with the cart support, the best solution was to use the RBE2 element. The latter is compatible both with supports and loads.

This configuration allowed to simulate the condition of the pin in which it is pushed down from the connecting rod and supported by the piston hubs. Using the maximum total force value, it was possible to verify the stress distribution along the pin in the worst possible condition.

It was finally possible to start the analysis. The non-linear analysis works with an *incremental simulation*. In the first step, the solver loads the components with a fraction of the total force value. If the simulation converges, the solver will increment (that's why is called "incremental") the force fraction and the process repeats over and over until the final value of the force is reached and the simulation concludes. This process explains the presence of "Load Factors" in the post-processor software *HyperView*. The *Load Factors* represents the increment of force applied in a certain step and they're expressed with the E-notation.

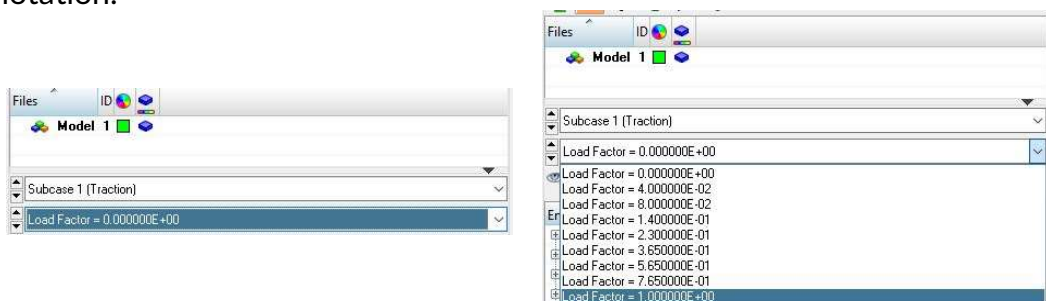


Figure IV. 2-19 Load Factors

The incremental step was automatically defined by the software but it could be also manually defined by the user.

### IV.2) 3. Altair Hypermesh – Layered Solid Shell using PSOLID

Since the PCOMPLS results couldn't be validated through visual verification, another model was prepared. The last model consisted of a layered solid wrist pin composed by PSOLID elements. These elements are the common choice in the solid components simulations. The limit to this model was represented by the impossibility to orient manually the material fibers through any of the Hypermesh tool. To make up for this problem a special script was exploited. The script, available at the Altair Connect page, is called "ElemSys1.tcl" and can be easily executed through Hypermesh, as shown in Figure IV. 2-20:

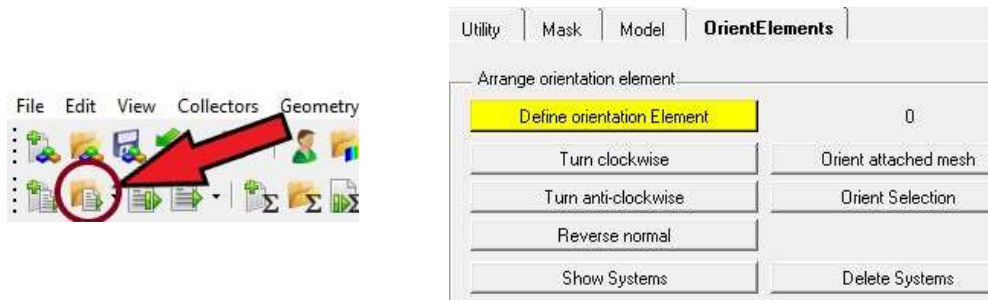


Figure IV. 2-20 Script Opening

This script made possible to change manually the orientation of the fibers inside the elements. Using the *CORDM* box (element reference system box) inside PSOLID property in order to change the material orientation was insufficient. It was possible to change the orientation before assigning the property to the components, but when the property was assigned the orientation changed.

The script allowed to choose a single element inside the mesh (Figure IV. 2-21), change the orientation of that element (Figure IV. 2-22) and then to assign the orientation to the attached mesh (Figure IV. 2-23). The steps are shown in the following figures:

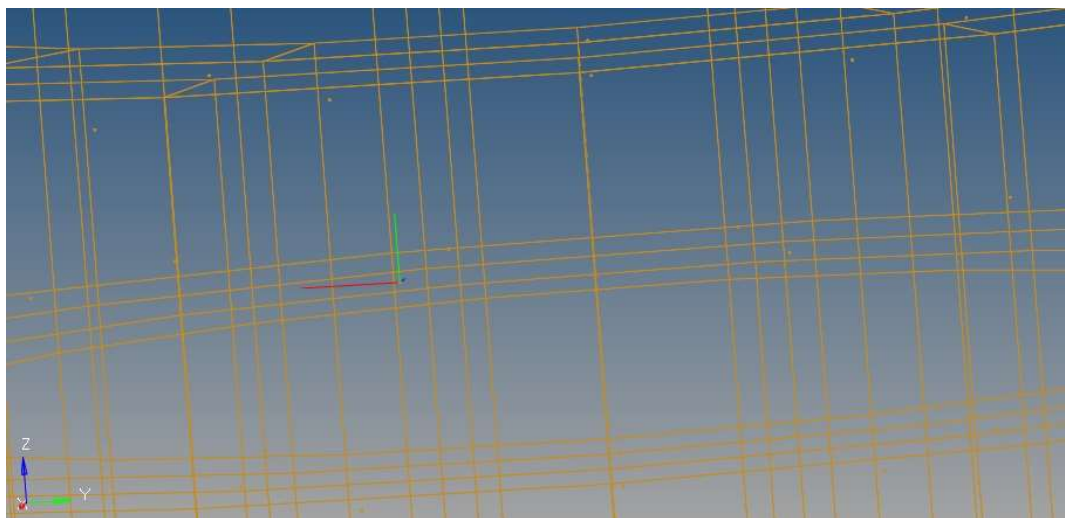


Figure IV. 2-21 Selection of the element

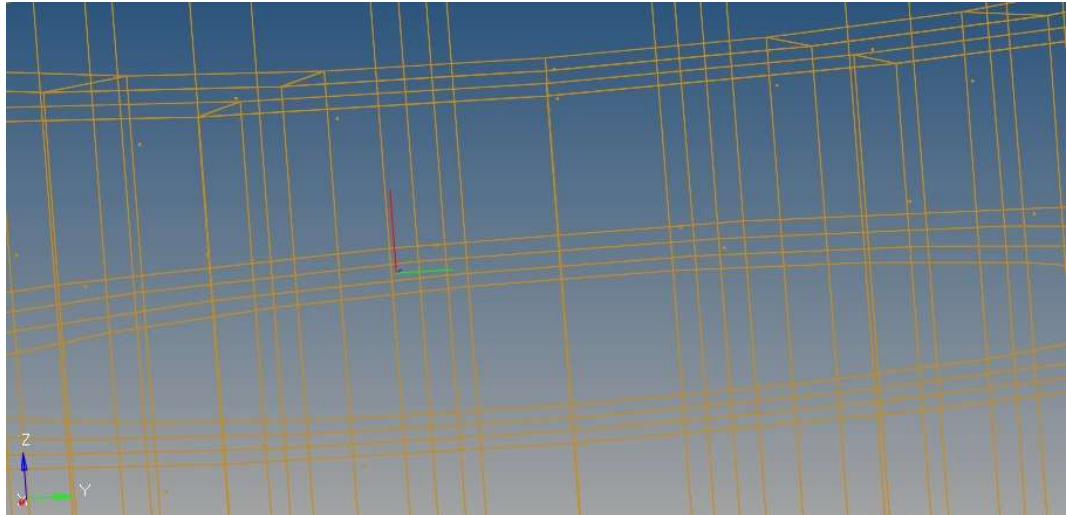


Figure IV. 2-22 Rotation of the fiber of the single element

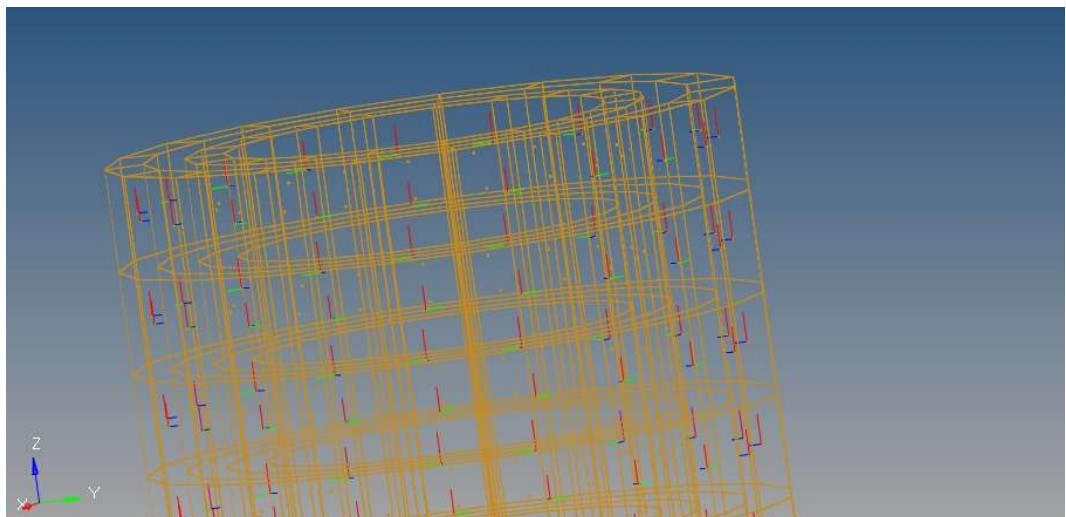


Figure IV. 2-23 Fiber alignment for the attached mesh

Once the orientation was defined, it was possible to visualize the orientation through the “Systems” subpanel in “Analysis”, as shown in Figure IV. 2-24:

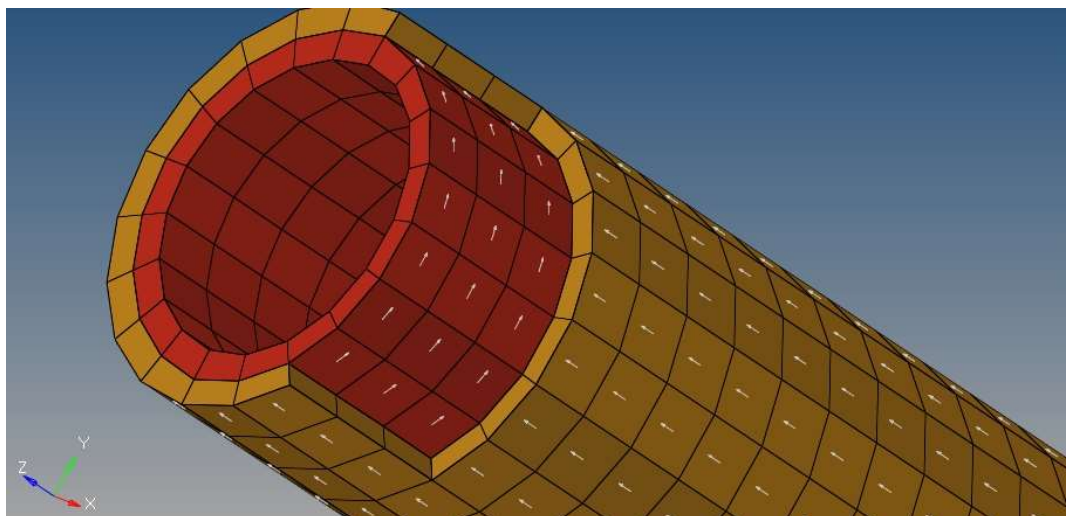


Figure IV. 2-24 Material Orientation through “Systems” subpanel(\*)

(\*) For simplicity, the Figure IV. 2-24 shows only a sample, not the final wrist pin model

Beside this benefit, the script shows some cons. The rotation of the fibers can be performed only by steps of  $\pm$  ninety degrees. The orientation of the attached mesh followed the mesh orientation of the selected element (the "Master Element"), but also the mesh of the overall geometry of the component. In this case, being the geometry very trivial, it was possible to decide easily the orientation of each layer. Other cases could presents come difficulties.

By using this tool, it was possible to make a comparison between the PCOMPLS layering and the PSOLID layering.

### IV. 3. Tsai-Wu Failure Criterion

Failure Index  $F$  is the an index needed to compare different solutions since it combines stress on different directions. As composite materials are the subjects of this project, a common failure index would fail. So an appropriate failure criterion must be chosen.

Tsai-Wu Failure Criterion was originally proposed for anisotropic materials. Subsequently the model was spread for orthotropic materials. The Tsai-Wu criterion is expressed through a quadratic polynomial expression of stresses with tensorial coefficients. The tensorial expressions allows a general applicability of the criterion to describe materials.

The most common form of the criterion employs the following failure function for orthotropic materials and its expressed in their principal axes:

$$F = F_{11}\sigma_1^2 + F_{22}\sigma_2^2 + F_{33}\sigma_3^2 + 2F_{23}\sigma_2\sigma_3 + 2F_{13}\sigma_1\sigma_3 + 2F_{12}\sigma_1\sigma_2 + F_1\sigma_1 + F_2\sigma_2 + F_3\sigma_3 + F_{44}\tau_{23}^2 + F_{55}\tau_{13}^2 + F_{66}\tau_{12}^2$$

Equation IV. 3-1 Tsai-Wu Failure Criterion

To deliver a failure criterion, it is claimed that the material is safe if  $F < 1$ , while the critical condition starts when  $F = 1$ .

It is generally unsatisfactory to consider laminated composites as an orthotropic material as far as their strength predictions are concerned, even if they exhibit orthotropic elastic behavior macroscopically. Unlike elastic properties which are dominated by the global behavior at a macroscale, strengths are governed by localized features at a micro level. Even in so-called non-local theories, it is still a local problem with a particular focus on a small neighborhood of the point of singularity.

Given a random distribution of fibers in the cross-section of an UD (Unidirectional) composite component, transverse isotropy is sufficiently satisfactory to describe the behavior of the UD composite, for which one has:

$$F_{33}=F_{22}; \quad | \quad F_{13}=F_{12}; \quad | \quad F_3=F_2; \quad | \quad F_{55}=F_{66}; \quad | \quad F_{23}=F_{22}-0.5F_{44}$$

Table IV. 3-1 Material Strengths

In this case the Tsai-Wu failure function can be reduced to:

$$F = F_{11}\sigma_1^2 + F_{22}(\sigma_2^2 + \sigma_3^2) + (2F_{22} - F_{44})\sigma_2\sigma_3 + 2F_{12}\sigma_1(\sigma_3 + \sigma_2) + F_1(\sigma_1 + \sigma_2) + F_2\sigma_3 + F_{44}\tau_{23}^2 + F_{66}(\tau_{13}^2 + \tau_{12}^2)$$

Equation IV. 3-2 Tsai-Wu Complete Failure Criterion

where the coefficients can be determined from the conventional strengths of UD composites as

$$F_{11} = \frac{1}{\sigma_{1t}^*\sigma_{1c}^*}; F_{22} = \frac{1}{\sigma_{2t}^*\sigma_{2c}^*};$$

$$F_1 = \frac{1}{\sigma_{1t}^*} - \frac{1}{\sigma_{1c}^*}; F_2 = \frac{1}{\sigma_{2t}^*} - \frac{1}{\sigma_{2c}^*};$$

$$F_{44} = \frac{1}{(\tau_{23}^*)^2}; F_{66} = \frac{1}{(\tau_{12}^*)^2}$$

Equation IV. 3-3 Tsai-Wu Failure Coefficients

with  $\sigma_{1t}^*$  and  $\sigma_{1c}^*$  being the tensile and compressive strengths of the material along fibers,  $\sigma_{2t}^*$  and  $\sigma_{2c}^*$  those in the direction transverse to the fibers, and  $\tau_{12}^*$  and  $\tau_{23}^*$  the shear strengths along and transverse to fibers. These strengths properties were supplied by the producer of the material.

Anyway, the coefficient  $F_{12}$  has not yet been specified and should be ideally determined through biaxial stress tests. Given the difficulties in conducting this type of tests, no standard method is available to determine it.

According with Tsai and Wu, the failure criterion gives rise to a closed ellipsoid. This condition can be employed to evaluate  $F_{12}$  coefficient.

For most applications under in-plane stresses Equation IV. 3-4 can be rewritten in its 2D form:

$$F = F_{11}\sigma_1^2 + 2F_{12}\sigma_1\sigma_2 + F_{22}\sigma_2^2 + F_{66}\tau_{12}^2 + F_1\sigma_1 + F_2\sigma_2$$

Equation IV. 3-4 Tsai-Wu Reduced Failure Criterion

As  $F_{12}$  is associated only with direct stresses  $\sigma_1$  and  $\sigma_2$ , some considerations can be made below when the material is subject to biaxial direct stresses. The critical condition can be simplified in this case to

$$F_{11}\sigma_1^2 + 2F_{12}\sigma_1\sigma_2 + F_{22}\sigma_2^2 + F_1\sigma_1 + F_2\sigma_2 = 1$$

Equation IV. 3-5 Tsai-Wu Reduced Criterion critical condition

This defines a typical conic section in the  $\sigma_1$ -  $\sigma_2$  plane. The condition for the failure locus in the  $\sigma_1$ -  $\sigma_2$  plane to be an ellipse is given largely as

$$F_{12}^2 < F_{11}F_{22}$$

Equation IV. 3-6  $F_{12}$  Critical Condition

However, this only defines a range for  $F_{12}$ , which appears to be rather wide in most cases. The complete determination of  $F_{12}$  remains as an issue to be resolved. It has been left as an empirical parameter. One form of it has been suggested as

$$F_{12} = -\frac{1}{2}\sqrt{F_{11}F_{22}}$$

Equation IV. 3-7  $F_{12}$  Evaluation

which was expressed in terms of conventional strength properties. The justifications for the particular form are:

- It falls in the range as defined by  $F_{12} = -\frac{1}{2}\sqrt{F_{11}F_{22}}$
- It allows itself to be degenerated to that of von Mises if the material is specialized to isotropic having equal tensile and compressive strengths.

The Equation IV. 3-4 can be plotted and it will be represented by an ellipse, as shown in Figure IV. 3-1. The four conventional strength properties ( $\sigma_{1t}^*$ ,  $\sigma_{1c}^*$ ,  $\sigma_{2t}^*$  and  $\sigma_{2c}^*$ ) represents the intersecting point of the ellipse with the coordinate axis. These four points aren't sufficient to determine univocally an ellipse. The interactive term  $F_{12}$  plays the role of providing another anchoring point so that the ellipse can be univocally determined. As it is possible to notice in *Figure IV. 3-1 Tsai-Wu ellipse*, different values of  $F_{12}$  tend to tilt the ellipse.

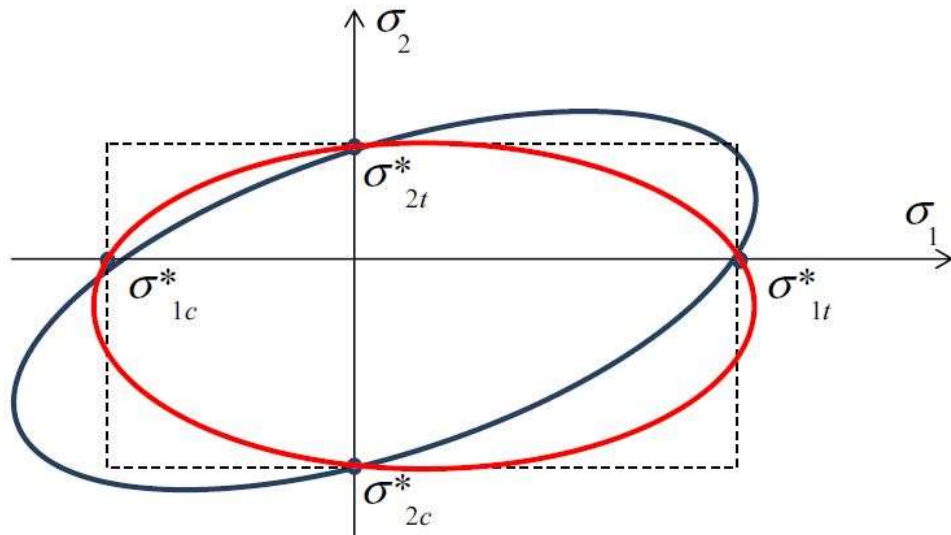


Figure IV. 3-1 Tsai-Wu ellipse

Unluckily, the criterion already explained couldn't be applied to the model in Hypermesh. Indeed, the software hasn't implemented the failure criterion for solid layered elements yet. Hyperview offers the possibility to implement manually the functions by writing the failure criterion equation through the panel "Derived Results". A derived result in Hyperview was tried in order to obtain a value for the Failure Index, but the result wasn't acceptable.

Probably this unsatisfactory result was caused by the not completed optimization of the solid layer model in Hypermesh (both with PCOMPLS and PSOLID elements).

A tentative of application of the Tsai-Wu Criterion was performed on a second Laminate model, this time as Semi-Complete Pin Model. The results of this model will be shown in the next chapter. The values are just indicative, since the pin is treated as a shell. The stress values of the simulation exceed the real values, evaluated on the solid layered components.

## V. Conclusions

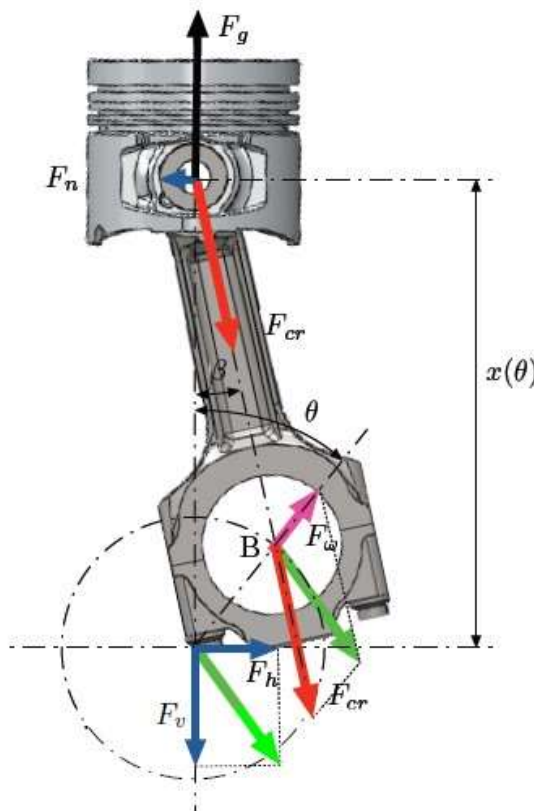
### V. 1. Consequences on engine

The introduction of lighters components inside the engine would bring to some benefits. The lower weights would cause a reduction of the inertial forces of each component allowing a more balanced engine.

As it was possible to see in Figure III. 3-2, the available torque at the crank shaft shows a benefit: the torque with composite material components has a higher peak value due to the lower inertial force. The inertial force effect is opposite to the gas pressure effect. The reduction of the inertial force plays a beneficial role in the generation of the torque, increasing its value during the combustion phase.

It was also possible to notice that the oscillation around the x-axis are lower in the case of the composite components with respect to the steel components. This is still linked to the lower inertial force.

From the engine block point of view, the forces on the block can be summarized in the following way:



$$\begin{cases} F_H = F_\omega \sin\theta \\ F_V = F_a - F_\omega \cos\theta \end{cases}$$

Equation V. 1-1 Engine Block Forces

The vertical force  $F_V$  does not depend on the gas pressure because the two forces  $F_g$ , one acting on the piston and one on the cylinder head, have equal value but opposite direction, cancelling each other.

Figure V. 1-1 Engine Block Forces

The introduction of composite components would lead to a considerable reduction of these forces on the engine block. Referring to the maximum values<sup>(\*)</sup> of  $F_V$  and  $F_H$ :

Steel		Composite		Reduction
$F_{H, Steel}$	14147 N	$F_{H, Composite}$	11234 N	20,58 %

$F_{V, Steel}$	19074 N	$F_{V, Composite}$	14800 N	22,41 %
$F_{Total, Steel}$	23747 N	$F_{Total, Composite}$	18581 N	21,76 %

Table V. 1-1 Engine Block Forces Comparison

(\*) since only the maximum values was used for the comparison, the reduction percentage can be seen as the maximum percentage of force reduction.

Consequence on the engine would lead to a smaller and lighter crankshaft, due to the reduced forces acting on it. Also, smaller and lighter crank-webs and flywheel due to the lower engine irregularity. Of course, these reductions would affect also the engine block and the bearings, that would be lighters since the forces would be reduced.

## V. 2. FEM Results

In this paragraph the results of the different simulation are presented. The graphical results will show not only the stress distribution for each model, but also the comparison between the different model discussed in the chapter IV. 2. Altair Hypermesh.

Regarding the Hyperview results, some clarifications should be done. The values showed in the results for the stress are in *MPa* and the strain in *mm*. To obtain *MPa* in Hyperview, proper measure units must be selected. The density was set in *tons/mm<sup>3</sup>* in the *Material card* and the forces were set in *N*. The supports are showed in order to provide a reference to the viewer. The rest of the components were hidden to allow the correct visualization of the results.

The principal stress directions are analyzed coherently to the following figure:

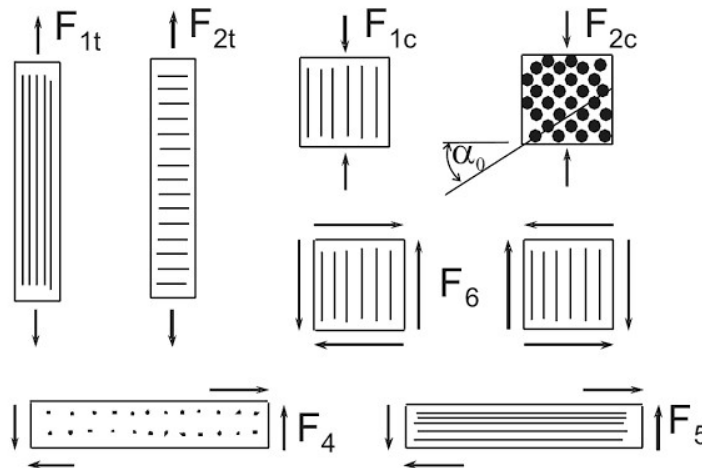


Figure V. 2-1 Principal Stress Directions

Where  $F_{1t}$  is the principal longitudinal stress and  $F_{2t}$  the principal transversal stress.

### V.2) 1. Laminated Wrist Pin

The results showed in this section are related to the model in Figure IV. 2-7. In fact, the results for the first laminated model, already showed in the

corresponding paragraph, were not so significant to be showed in this crucial section.

The Laminated Model was analyzed with the same characteristics of the Solid Layered Models in terms of loads, constraints and plies orientation.

The results for the Laminate Wrist Pin won't be discussed in a detailed way since the values won't be acceptable at all.

### Maximum Displacements:

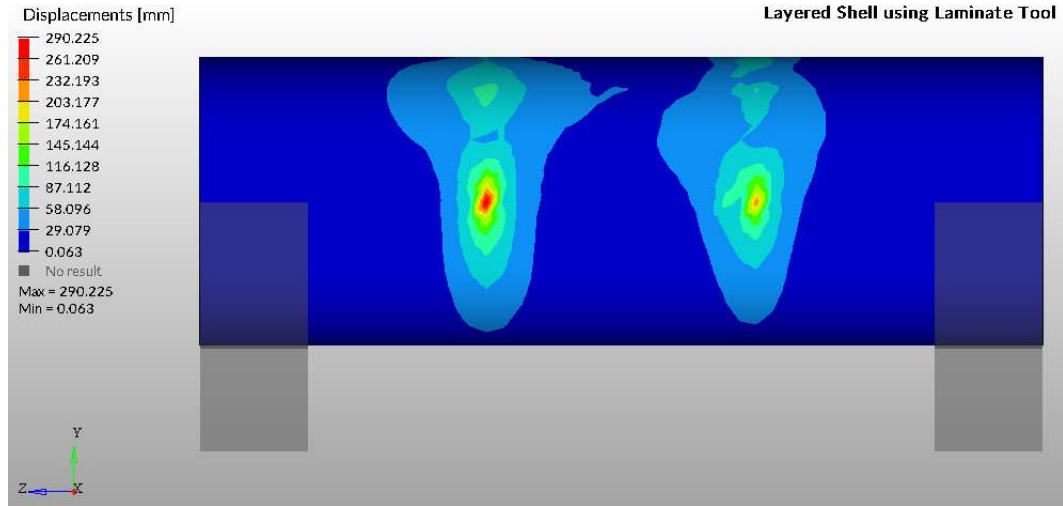


Figure V. 2-2 Laminated Pin Displacement Lateral View

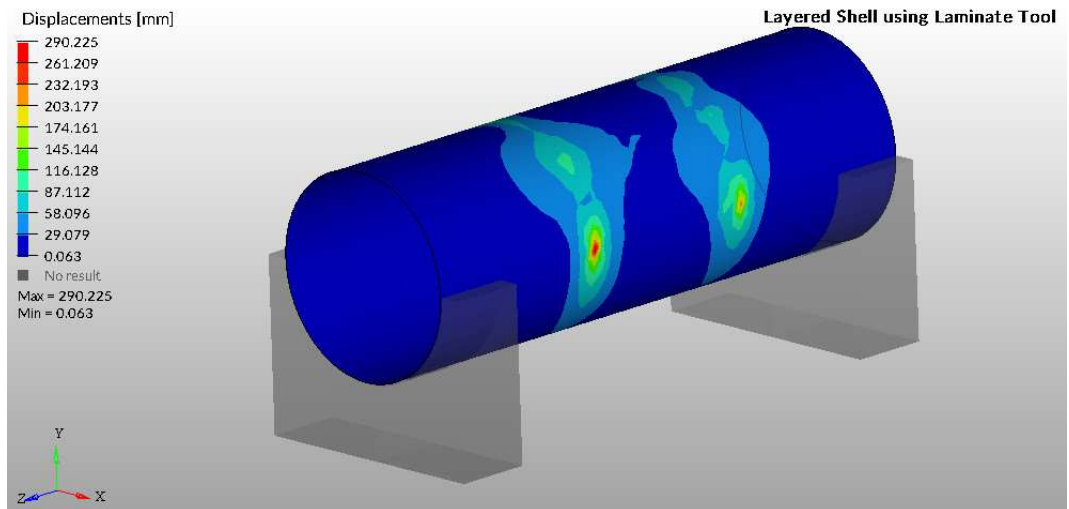


Figure V. 2-3 Laminated Pin Displacement Top View

As it is possible to notice the values of the displacements are not acceptable, the maximum value is equal to 290 mm. This is due to the shell elements used in this model. The shell elements loaded with about 24 kN of force are really stressed.

### Principal Stress – Direction 1:

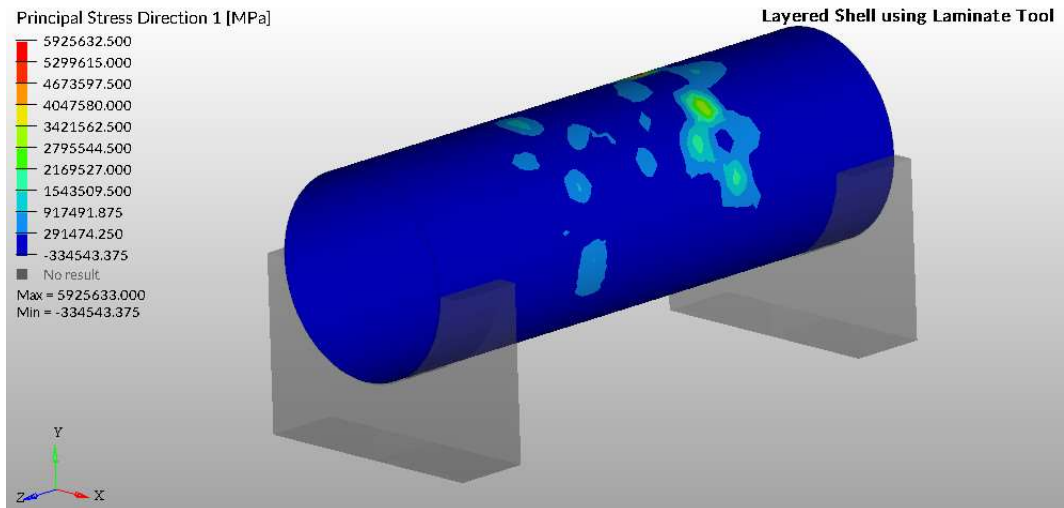


Figure V. 2-4 Laminated Pin Principal Stress Direction 1 Top View

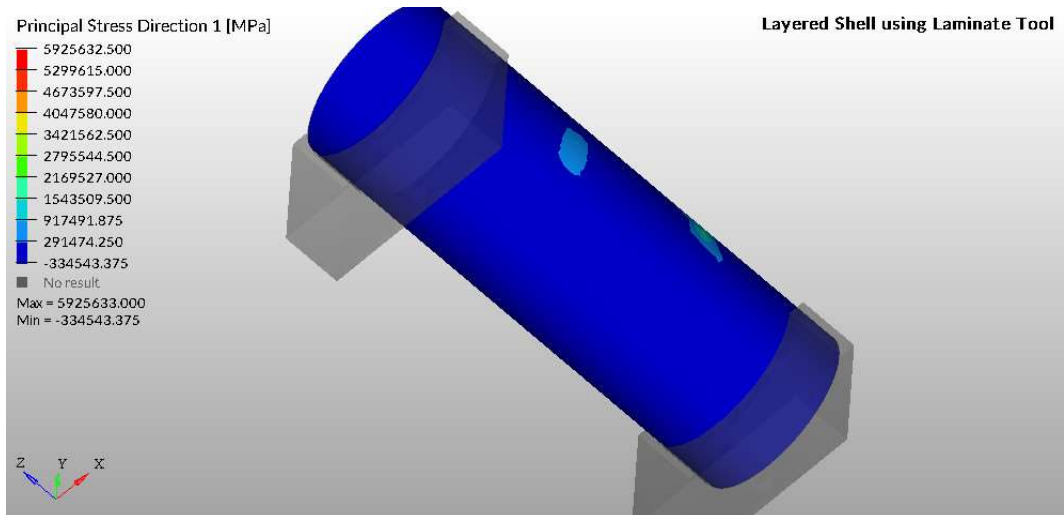


Figure V. 2-5 Laminated Pin Principal Stress Direction 1 Bottom View

Also in this case it is possible to notice that the values of the stress aren't acceptable. When the next model results will be discussed, it will be possible to notice that the order of magnitude in the Laminated Model is six times higher than the Solid Models.

### Principal Stress – Direction 3:

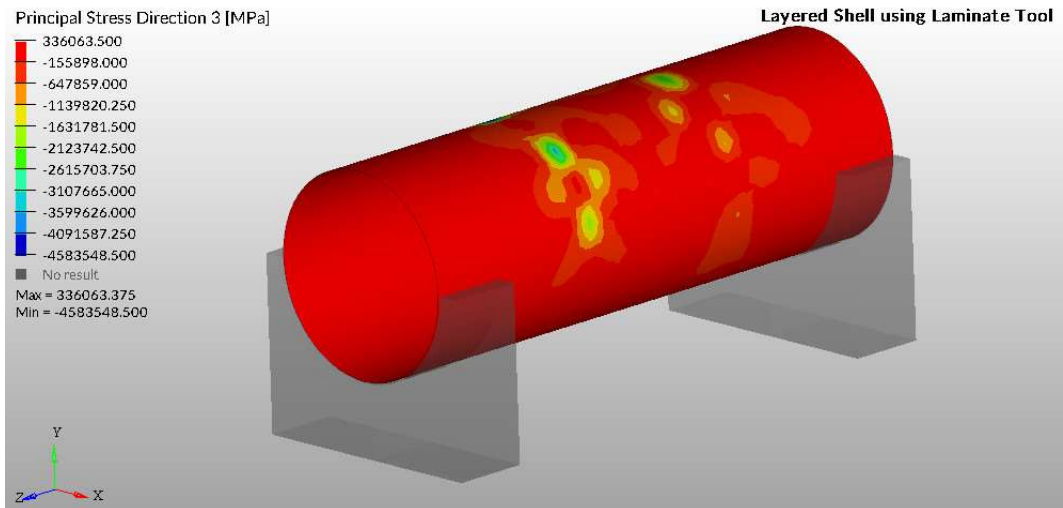


Figure V. 2-6 Laminated Pin Principal Stress Direction 3 Top View

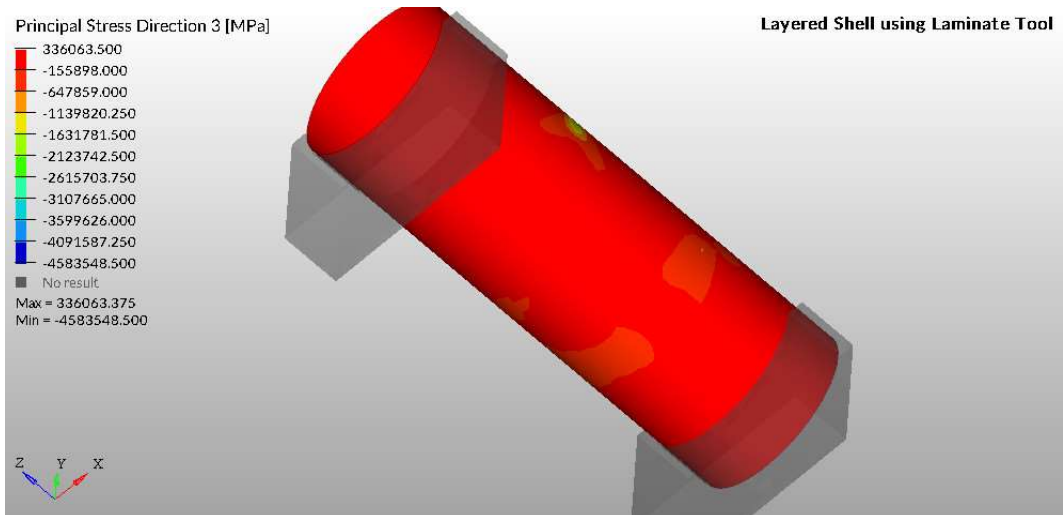


Figure V. 2-7 Laminated Pin Principal Stress Direction 3 Bottom View

The software didn't allow to choose the P2 direction for the principal stress, so it won't be reported in this section. Next stress will be the Shear Stress.

### Shear Stress:

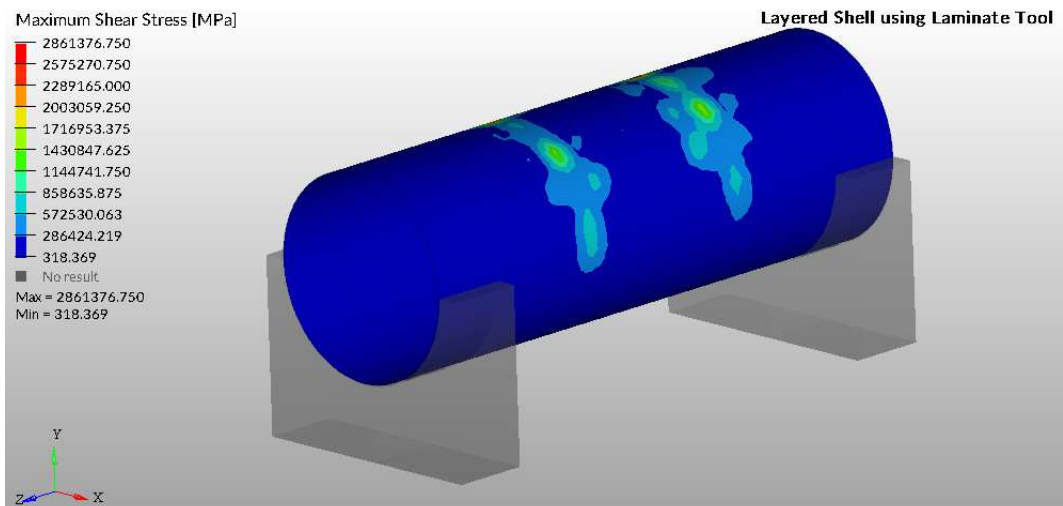


Figure V. 2-8 Laminated Pin Shear Stress Top View

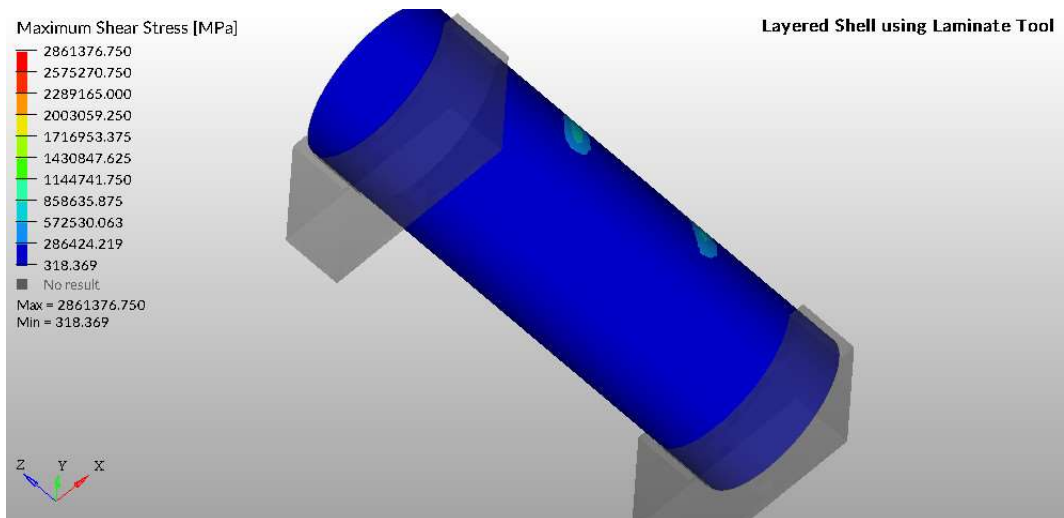


Figure V. 2-9 Laminated Pin Shear Stress Bottom View

**Composite Failure Index (Tsai-Wu):**

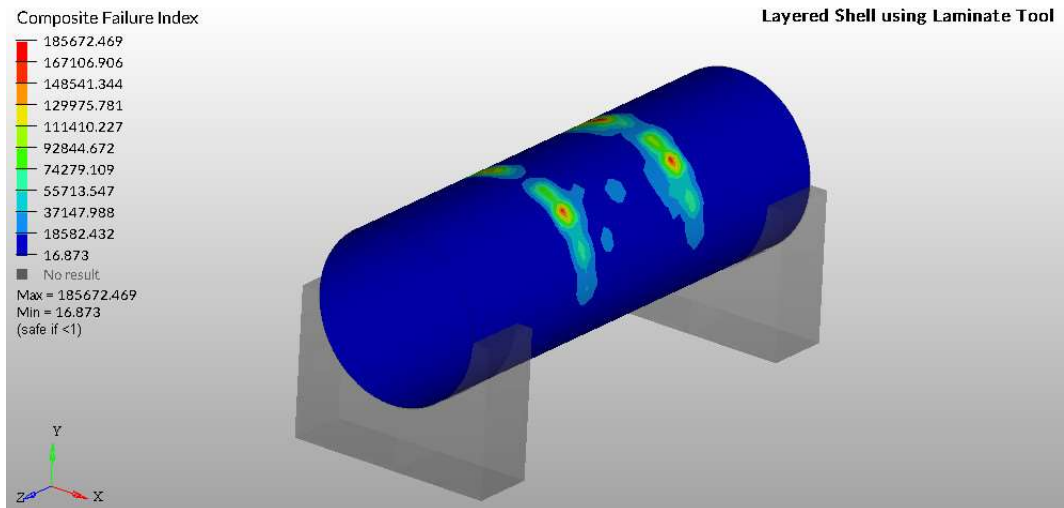


Figure V. 2-10 Laminated Pin Failure Index Top View

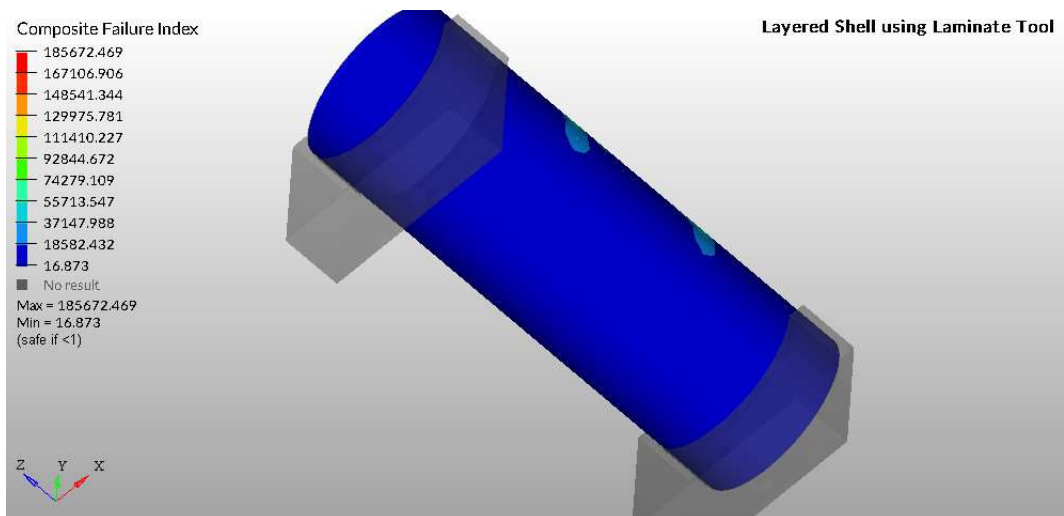


Figure V. 2-11 Laminated Pin Failure Index Bottom View

The Composite Failure Index wasn't acceptable at all. Even the lowest value is considerably higher than 1 (limit value to be safe).

The weaknesses of the software were showed in this paragraph, since the use of the shell elements wasn't appropriate for this kind of components. It is finally possible to say that the use of the Laminate Tool for this kind of application is not suggested. Next paragraphs will show the results for the Solid Layered Models.

## V.2) 2. PCOMPLS Solid Layer Wrist Pin

The results for the PCOMPLS model are showed.

### Maximum Displacement:

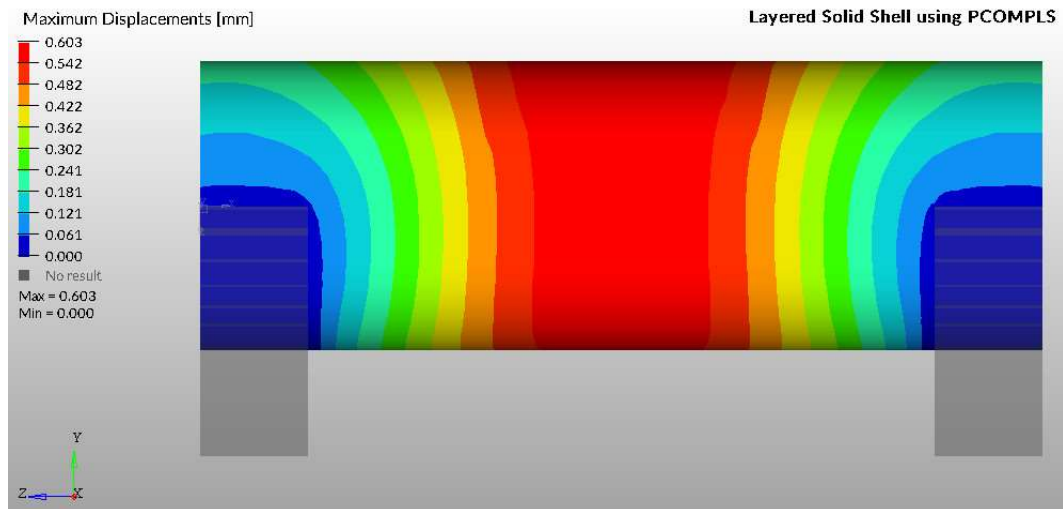


Figure V. 2-12 PCOMPLS Wrist Pin Displacement Lateral View

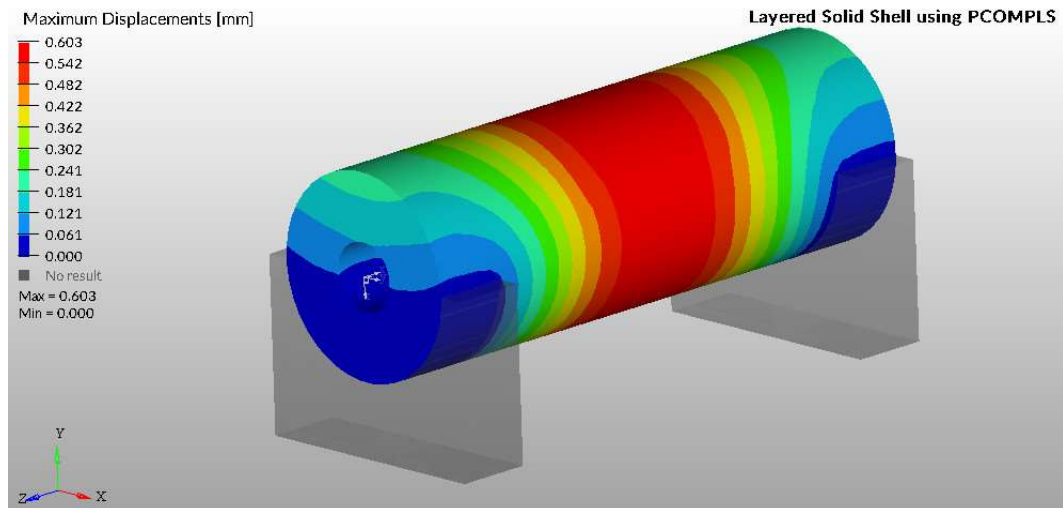


Figure V. 2-13 PCOMPLS Wrist Pin Displacement Top View

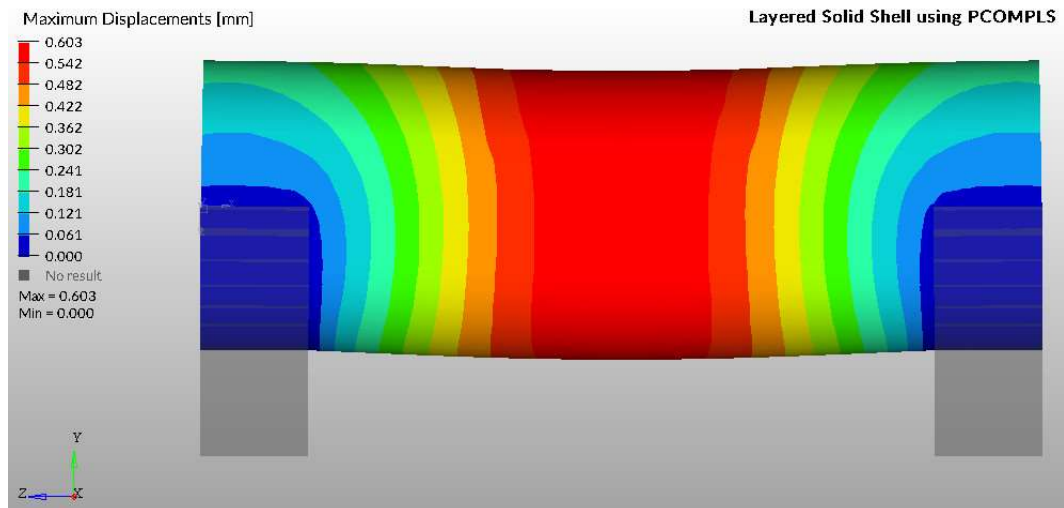


Figure V. 2-14 PCOMPLS Wrist Pin Displacement Lateral View after Load Application

The displacement distribution is symmetric, and the maximum value is equal to 0.606 mm. The value should be validated with a future CFD simulation to verify that this value wouldn't affect the lubrication negatively and with dynamic simulations to verify the presence or not of interferences. These interferences could cause seizure of the rotating components.

The maximum displacement obviously occurs at the center of the pin because in that portion the connecting rod push down the pin.

In Figure V. 2-14 it's possible to see the deformed pin after the application of the load. It can be notice that the pin tends to be bent. With this in mind it is finally possible to understand the importance of the longitudinal fibers' direction. These fibers will react to bending stress.

The stresses will be discussed in two layers, the layer called "Maximum Layer" showing the maximum stress values and the layer called "Minimum Layer" showing the minimum stress values. The Figures proposed in the following will show only the maximum possible value for the stress in absolute value: maximum layer will be taken for the tense regions and minimum layer will be taken for the compressed regions.

It is possible to notice the symmetry of the distribution, due to the geometrical symmetry of the model.

### Principal Stress – Longitudinal Direction:

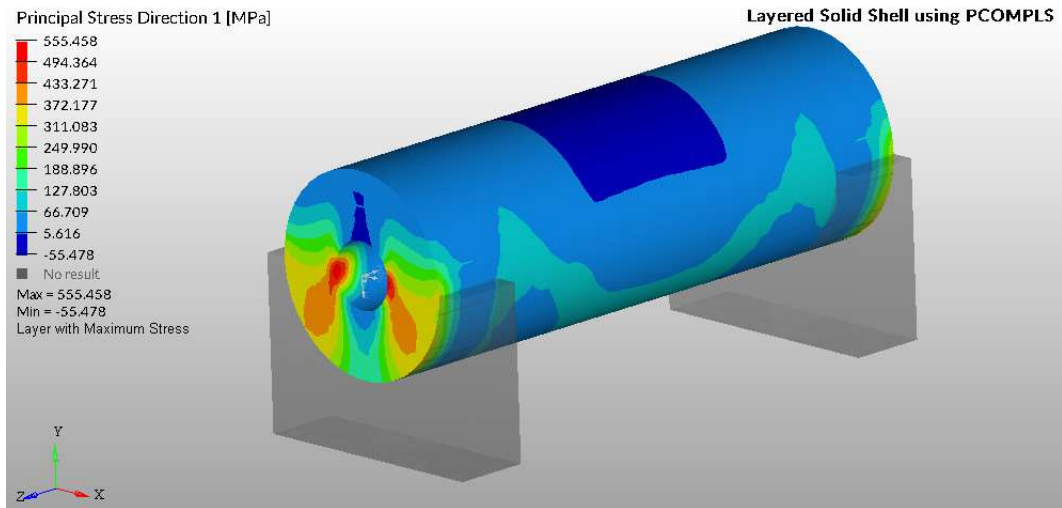


Figure V. 2-15 PCOMPLS Pin Principal Stress Direction 1 Top View - Maximum Layer

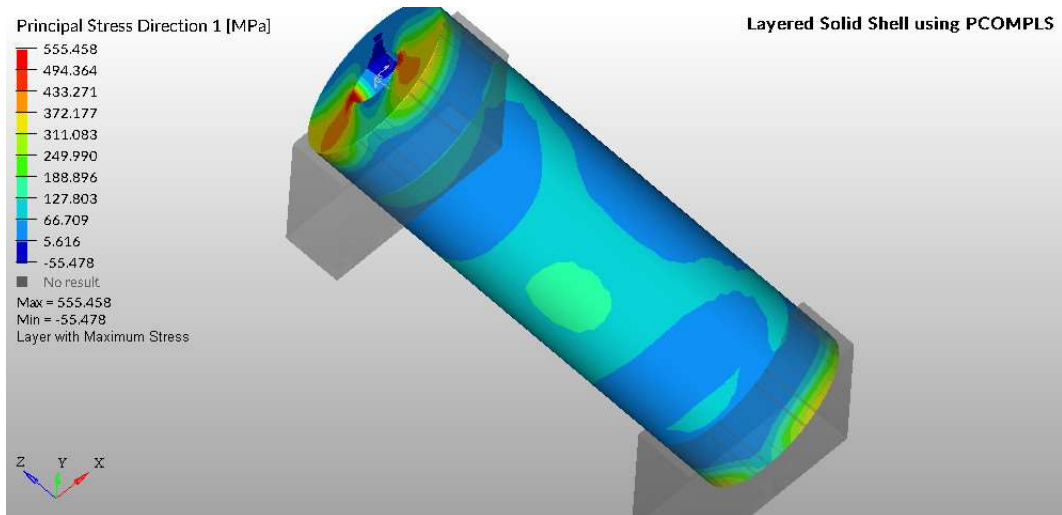


Figure V. 2-16 PCOMPLS Pin Principal Stress Direction 1 Bottom View - Maximum Layer

Considering the layer with the maximum stress values, the maximum value for the principal stress is equal to 555,46 MPa. The minimum value is equal to -55,48 MPa. These values mean that the red zones are pull, while the dark blue zones are compressed. These values should be validated through some tests in order to verify the resistance of the component. These values wouldn't bring to a failure since the longitudinal resistance of the material is equal to 2176 MPa.

It can be noticed that the most stressed region is the one near the central hole, so attention should be put in the design of that region. Except that zones, the rest of the pin is slightly stressed.

### Principal Stress – Transversal:

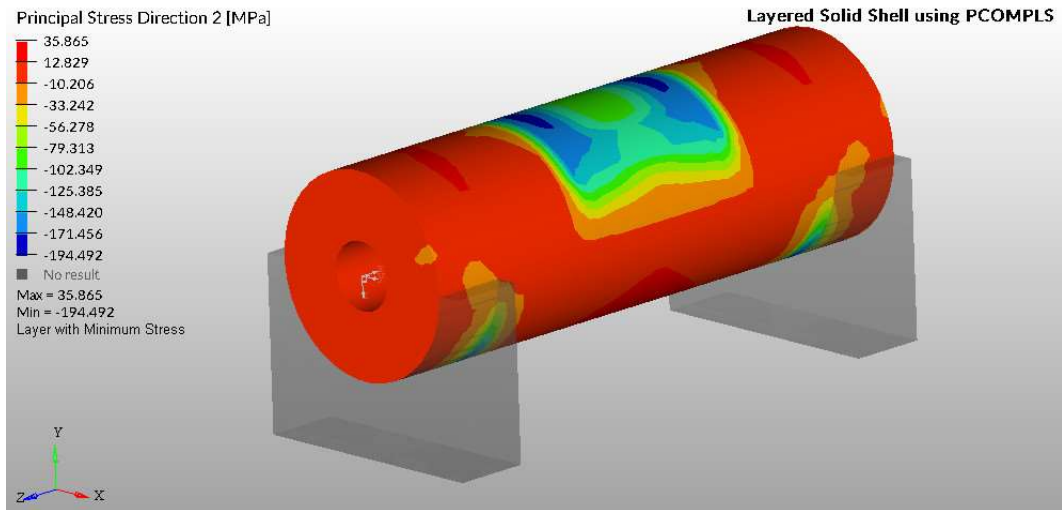


Figure V. 2-17 PCOMPLS Pin Principal Stress Direction 2 Top View - Minimum Layer

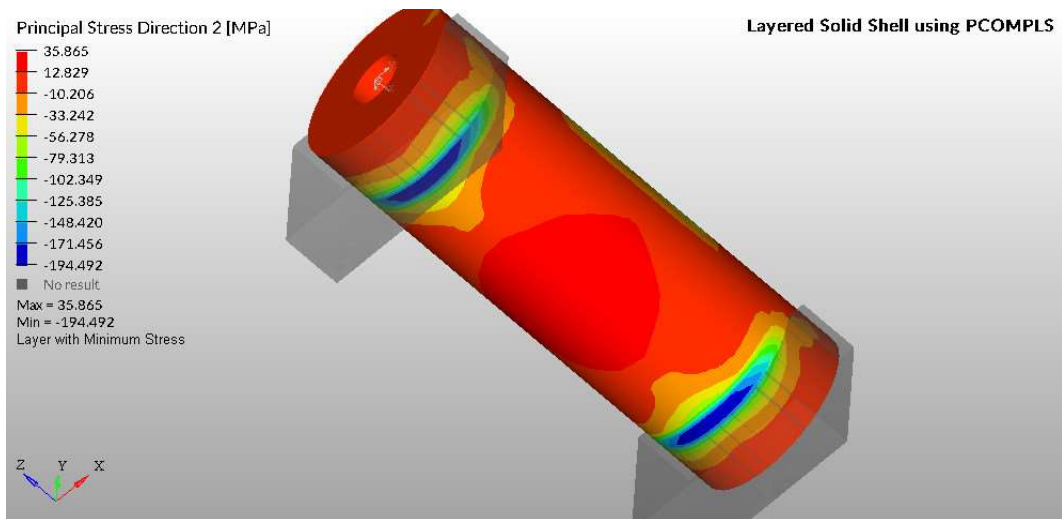


Figure V. 2-18 PCOMPLS Pin Principal Stress Direction 2 Bottom View - Minimum Layer

In this case it is possible to see a “more common” principal stress distribution with a compression state in the top center region, due to the presence of the connecting rod, and a traction state in the bottom center region. This distribution is the common distribution when bending is present: one region is compressed and the other is pull.

Attention should be put also on the region of the pin in contact with the piston hubs. Indeed, this region is also subject to a compressive state with the maximum compressive stress value. The more compressed region around the piston hubs occurs at the edge of the hubs themselves. This is probably due to the flection of the piston around the edge of the hubs.

Since transversal direction is characterized by a compressive state, the minimum layer was considered in this case. This can be explained thinking to the layers' distribution: the external layers material is stressed and tends to push the internal layers material. This effect is repeated over and over through the different layers starting from the most external through the most internal one.

### Principal Stress – Transversal:

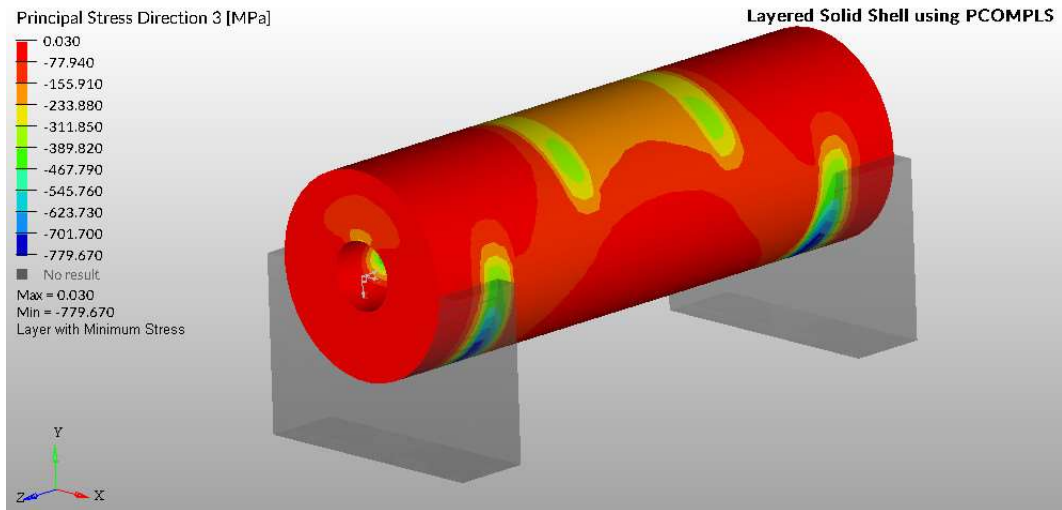


Figure V. 2-19 PCOMPLS Pin Principal Stress Direction 3 Top View - Minimum Layer

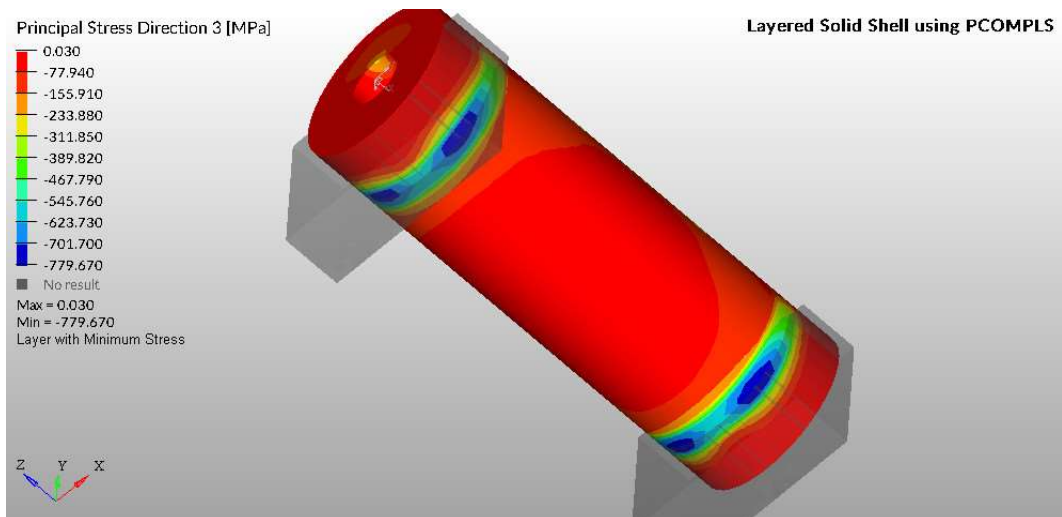


Figure V. 2-20 PCOMPLS Pin Principal Stress Direction 3 Bottom View - Minimum Layer

The stresses along the third direction show how important is the compressive state inside the pin. For this reason, the minimum layers was considered in this case. The traction value (positive maximum value) is almost negligible, while the compressive value is really high: its value is equal to -779,667 MPa (in the minimum layer) and to -329,33 MPa (in the maximum layer). Even in this case the most compressed region is the one near the piston hubs, where the edges of the hubs press the pin material. Considering the transversal resistance of the component, it is expected a failure of the component.

Next figures will show the Shear Stress state of the pin. This part is probably the most critical one, since the shear tends to make the different layers slide each other. The composite material layers are kept together by an Epoxy matrix. The shear stress is critical just for the matrix.

**Shear Stress:**

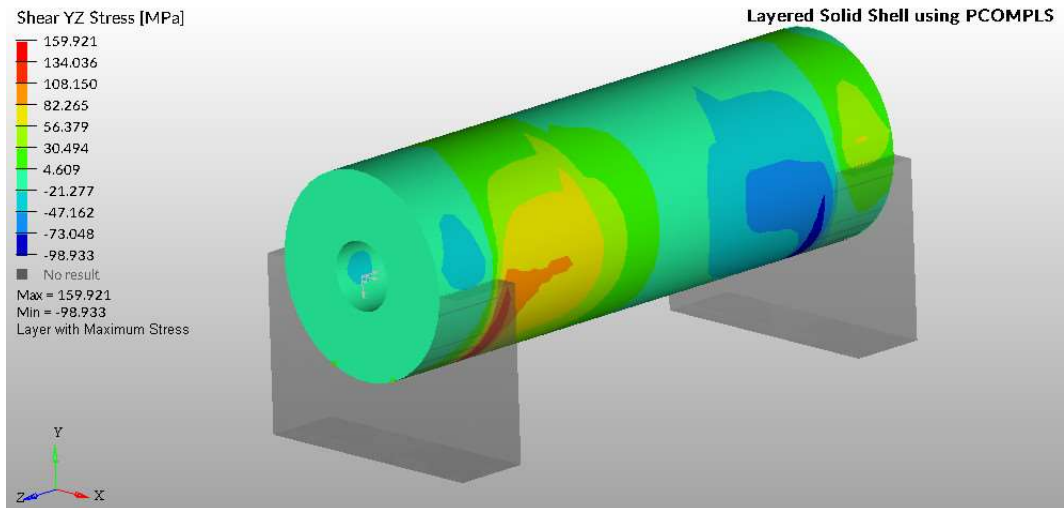


Figure V. 2-21 PCOMPLS Pin Shear Stress Top View - Maximum Layer

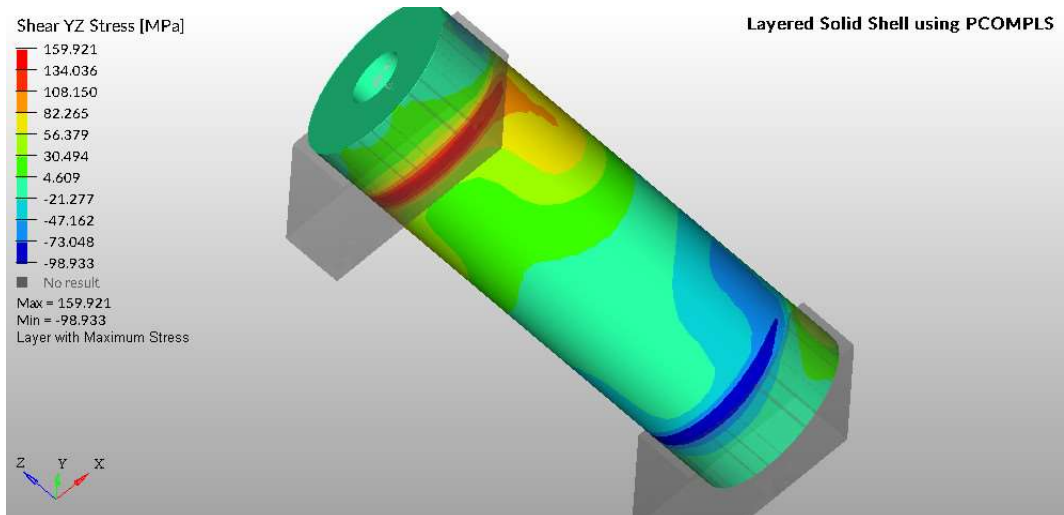


Figure V. 2-22 PCOMPLS Pin Shear Stress Bottom View - Maximum Layer

Considering that the material maximum shear stress is 140 MPa, the values showed in the results are quite always higher. This situation should lead to a failure of the component. Even if not present in the software, the Tsai-Wu Failure Index would probably overcome the value of 1. The principal stress along the longitudinal direction is acceptable, the real problem are the high shear stress values, considerably higher than the resistance of the material, and the transversal principal stress, in both case higher than the material resistance.

**V.2) 3. PSOLID Solid Layer Wrist Pin**

The results for the PSOLID model are showed. All the considerations done for the PCOMPLS regarding the stress and displacement distribution are still valid. A comparison will be performed in the next paragraph to show the differences between the two model results.

In this paragraph the results will be only showed, no comments will be present after each result. The final discussion will be proposed in the paragraph Comparison between PCOMPLS and PSOLID.

**Maximum Displacement:**

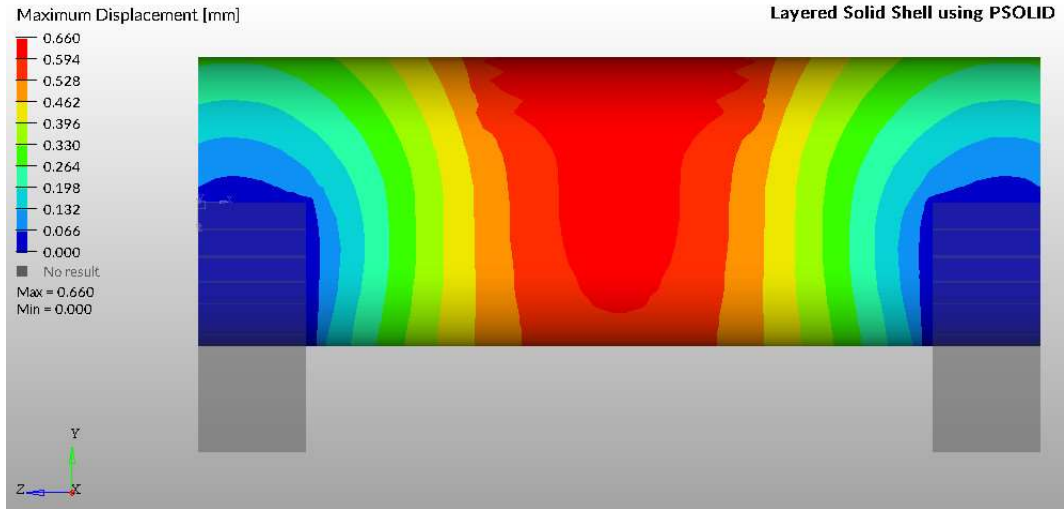


Figure V. 2-23 PSOLID Wrist Pin Displacement Lateral View after Load Application

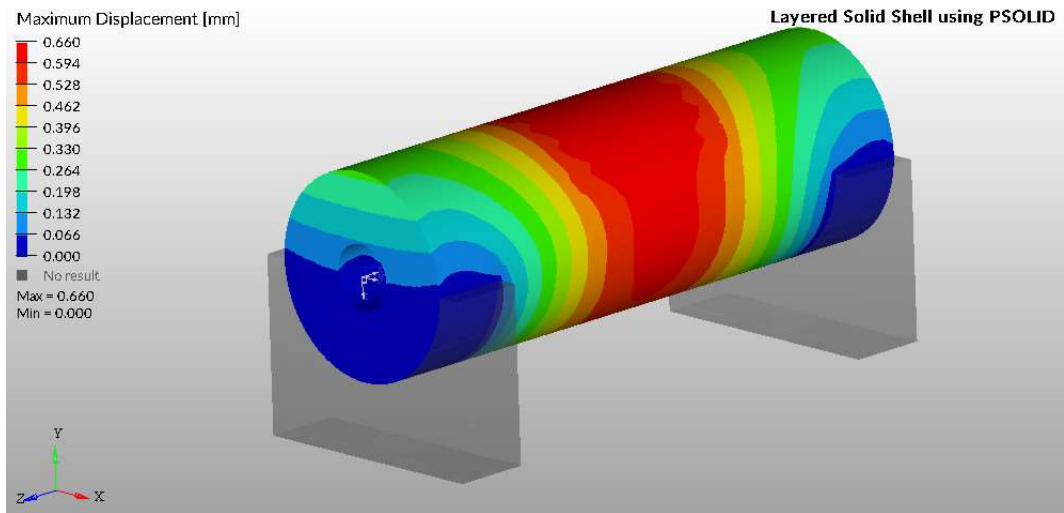


Figure V. 2-24 PSOLID Wrist Pin Displacement Top View

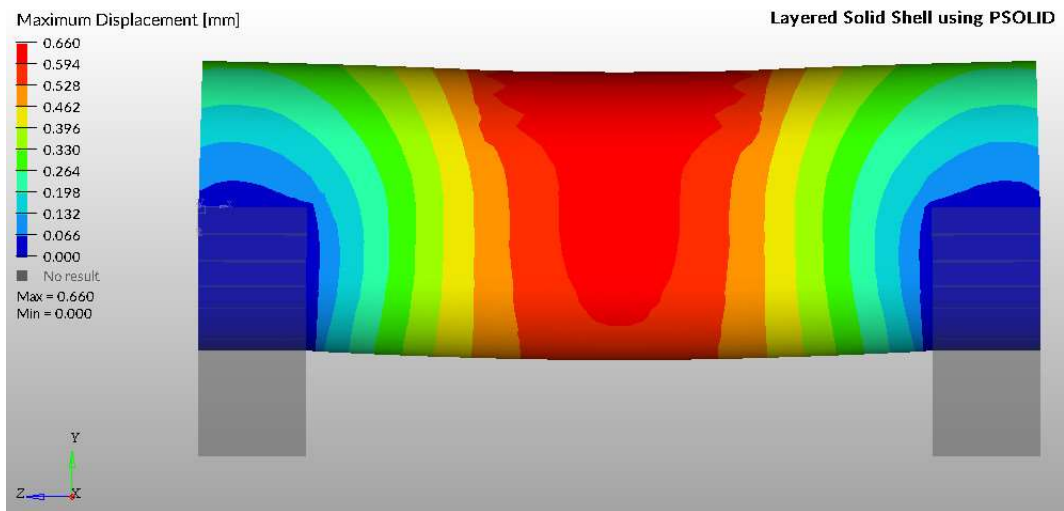


Figure V. 2-25 PSOLID Wrist Pin Displacement Lateral View after Load Application

**Principal Stress – Direction 1:**

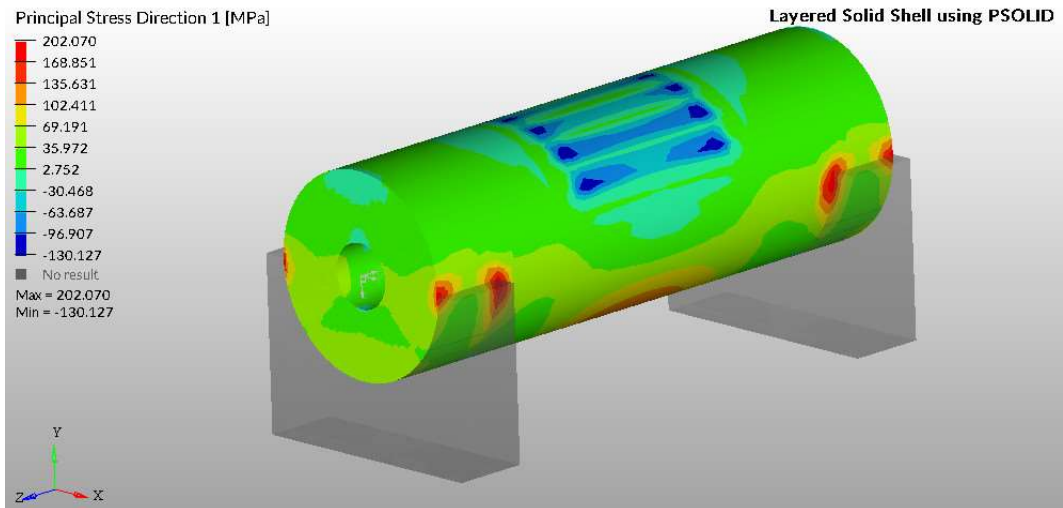


Figure V. 2-26 PSOLID Pin Principal Stress Direction 1 Top View

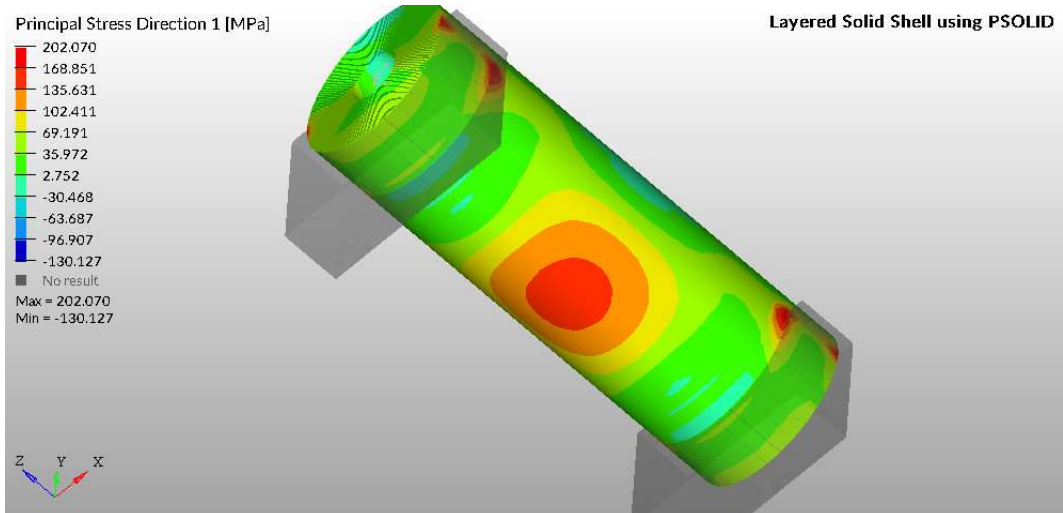


Figure V. 2-27 PSOLID Pin Principal Stress Direction 1 Bottom View

**Principal Stress – Direction 2:**

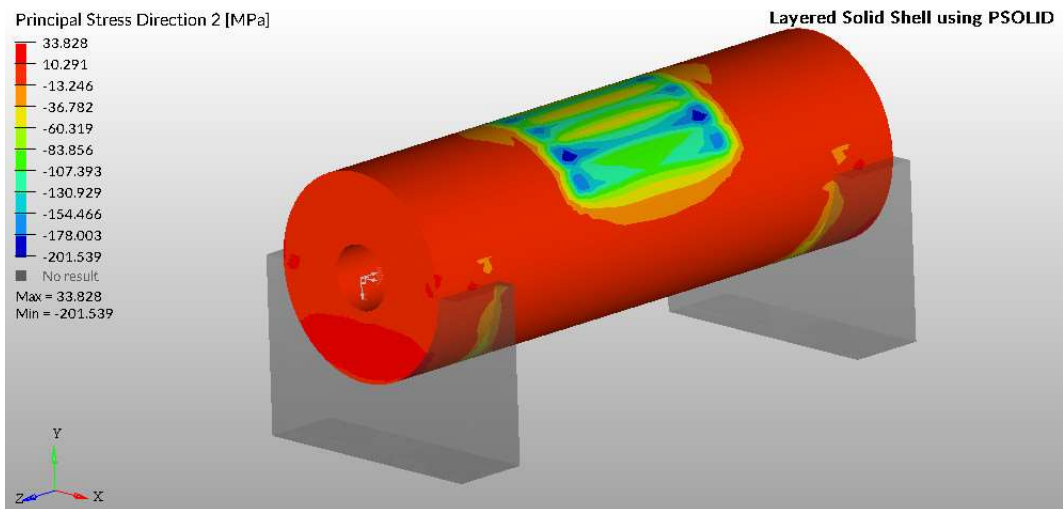


Figure V. 2-28 PSOLID Pin Principal Stress Direction 2 Top View

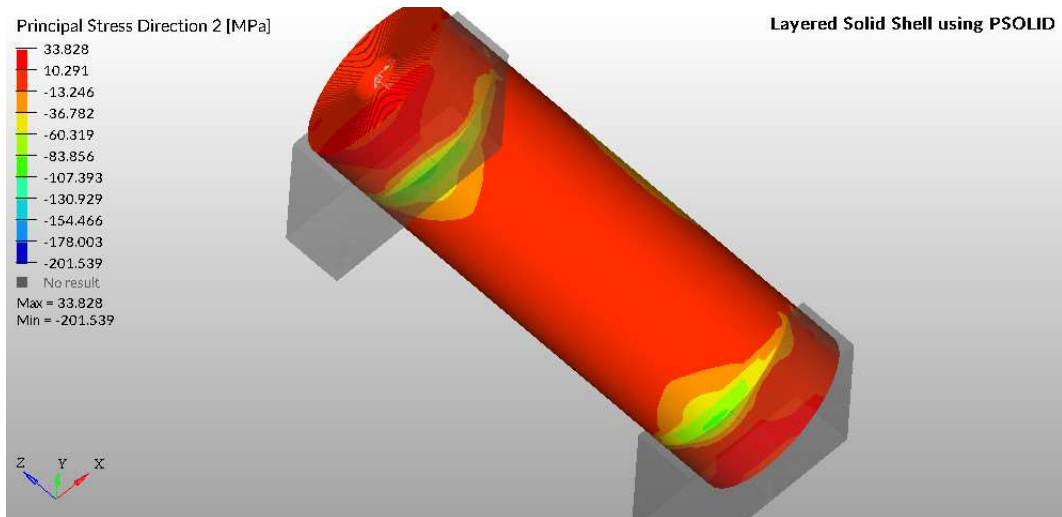


Figure V. 2-29 PSOLID Pin Principal Stress Direction 2 Bottom View

**Principal Stress – Direction 3:**

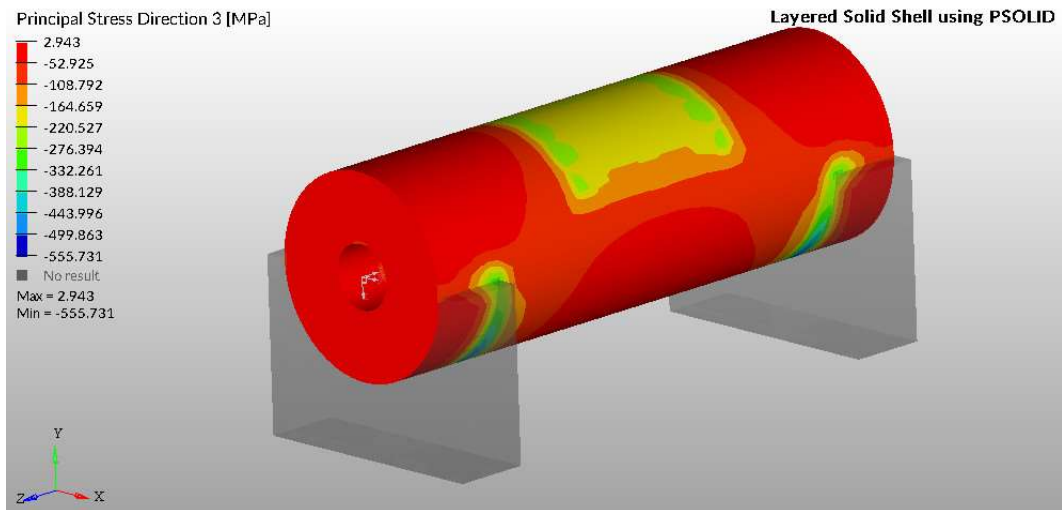


Figure V. 2-30 PSOLID Pin Principal Stress Direction 3 Top View

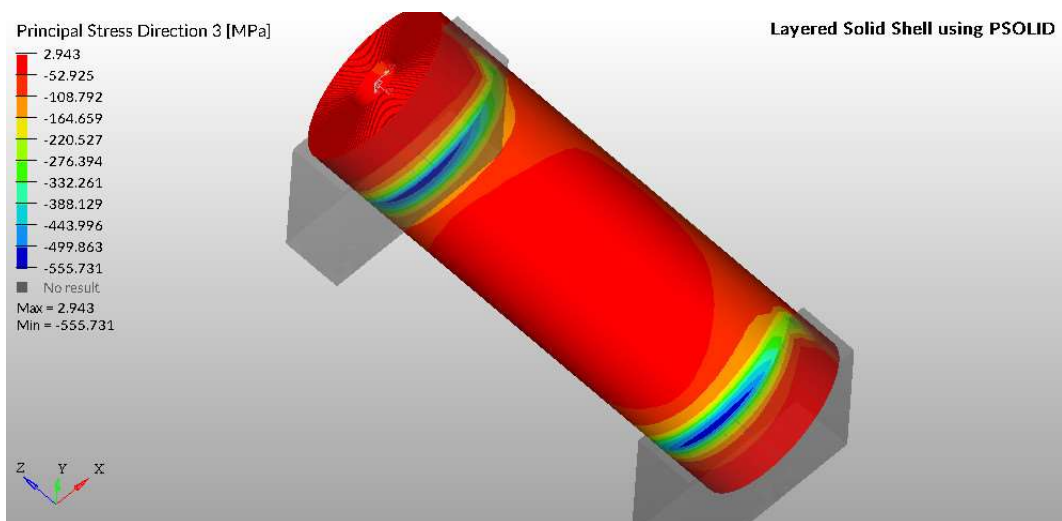


Figure V. 2-31 PSOLID Pin Principal Stress Direction 3 Bottom View

The two principal stresses along transverse directions demonstrate the most critical condition for the pin. In both direction 2 and 3, the maximum values of compression overcome the maximum transversal stress  $F_{2t}$  of 46,7 MPa.

### Shear Stress:

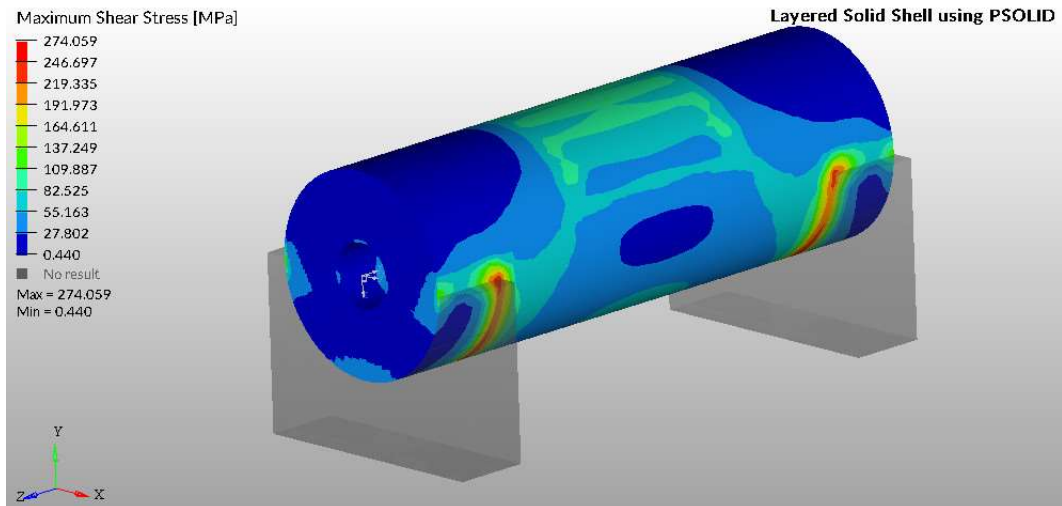


Figure V. 2-32 PSOLID Pin Shear Stress Top View

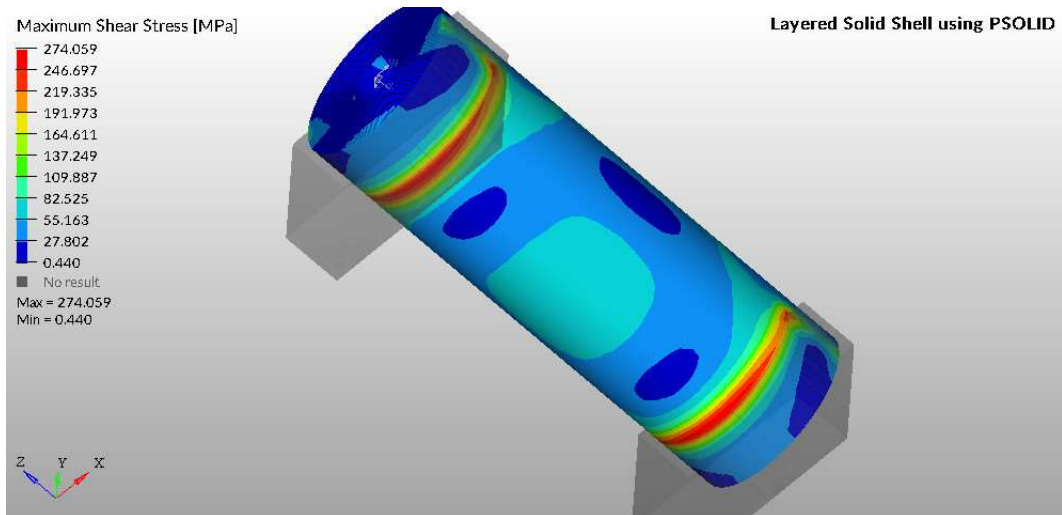


Figure V. 2-33 PSOLID Pin Shear Stress Bottom View

The shear stress distribution shows a concentration of the shear around the edges of the piston hubs. These regions represent a critical region for the component, with a high risk of failure.

The maximum value of the shear is 274,06 MPa, considerably higher than the maximum shear resistance of the material (140 MPa). From this result it possible to expect a failure.

#### V.2) 4. Comparison between PCOMPLS and PSOLID

The results of the PCOMPLS showed the real limit of this kind of property. At the actual state of art, the implementation of the software is really low, and the results are still not very representative of the actual case. The PSOLID, initially introduced as a pure comparison model, is indeed the more realistic model inside this project.

The results of the two models will be compared in the following and the differences will be discussed.

### Maximum Displacement:

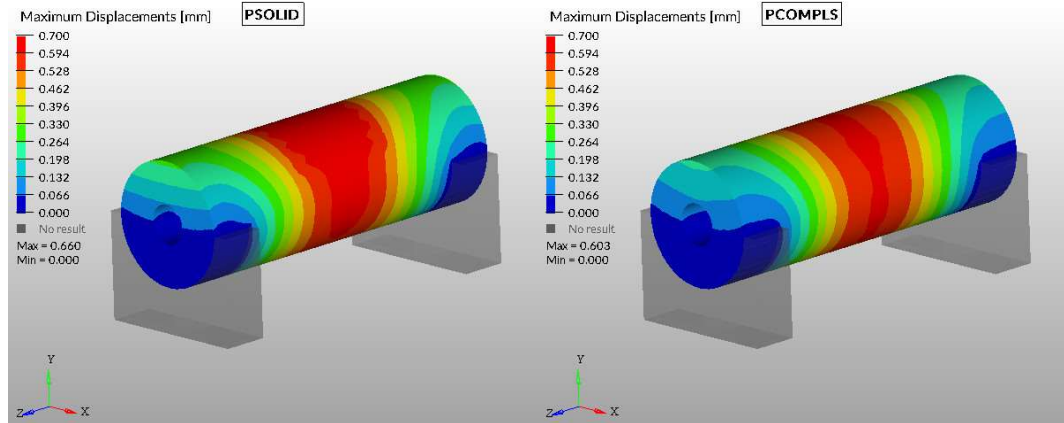


Figure V. 2-34 Displacements Comparison Top View

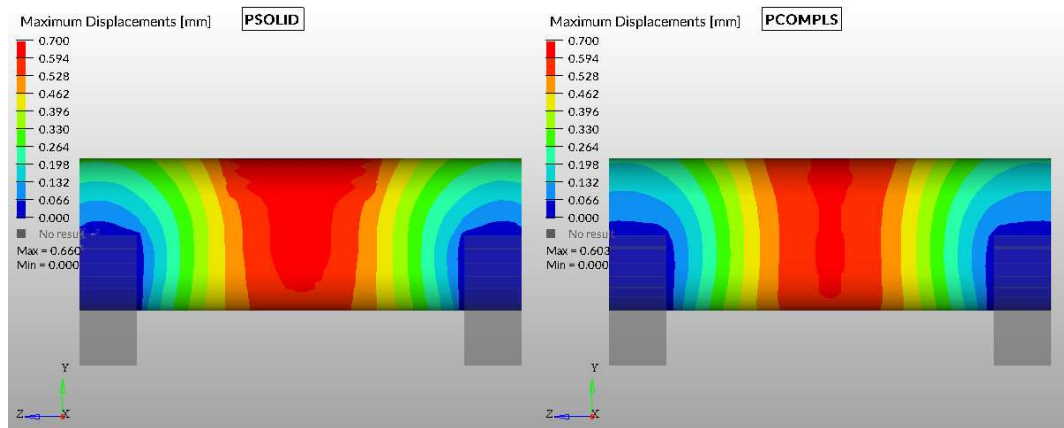


Figure V. 2-35 Displacements Comparison Lateral View

The displacements are more or less the same, both in terms of distribution and absolute value. The PSOLID model shows a slightly higher maximum deformation than the PCOMPLS model. In the PSOLID model it's possible to notice a higher spread of the deformation from the central region. In both cases, the maximum value of deformation rounds around the  $0.603 \div 0.660$  mm. These values should be properly validated through a CFD analysis to verify the correct lubrication and through another geometrical analysis to verify the correct coupling of the components without interference.

### Principal Stress – Direction 1:

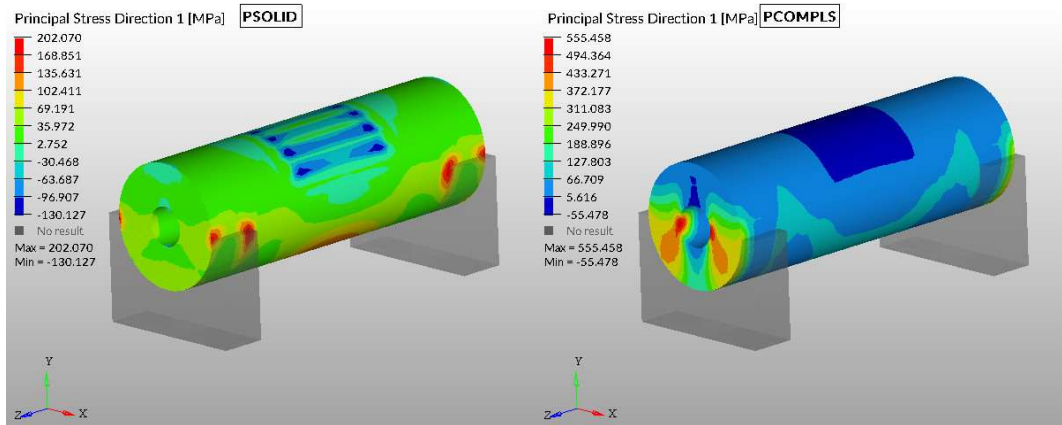


Figure V. 2-36 Principal Stress Direction 1 Comparison Top View

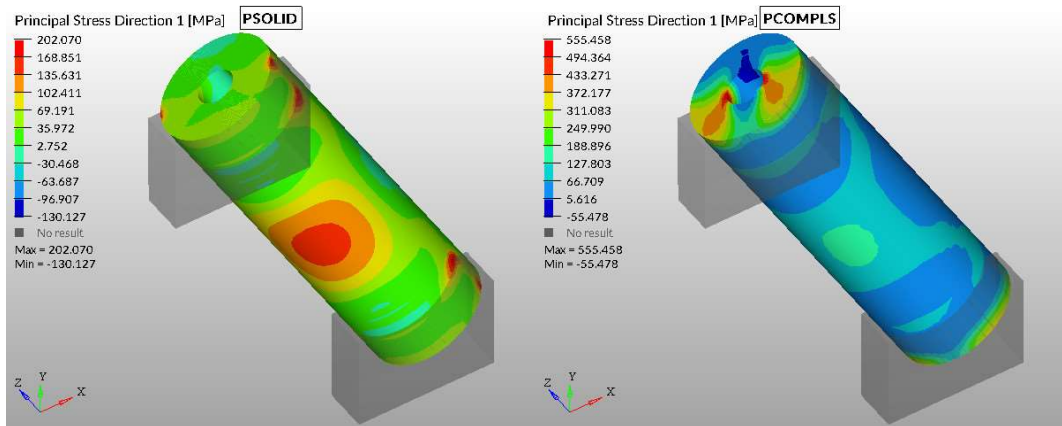


Figure V. 2-37 Principal Stress Direction 1 Comparison Bottom View

The principal stress distribution along the longitudinal direction show the real difference between the models. As it is possible to notice the distribution are totally different.

Also the values are different. Higher maximum value occurs in the PCOMPLS model. In both cases the maximum longitudinal resistance of the material is not reached. PSOLID model shows a higher compressive stress value (-130,13 MPa) than the PCOMPLS model (-55,48 MPa). Considering a longitudinal compressive resistance  $F_{1c}$  equal to the 80% of the longitudinal traction resistance  $F_{1t}$ :

$$F_{1c} = 80\% (F_{1t}) = 80\% (2176 \text{ MPa}) = 1740,8 \text{ MPa}$$

Equation V. 2-1 Longitudinal Compressive Resistance

The component, considering the longitudinal direction, won't fail. Different conclusions will be shown in the next results.

### Principal Stress – Direction 2:

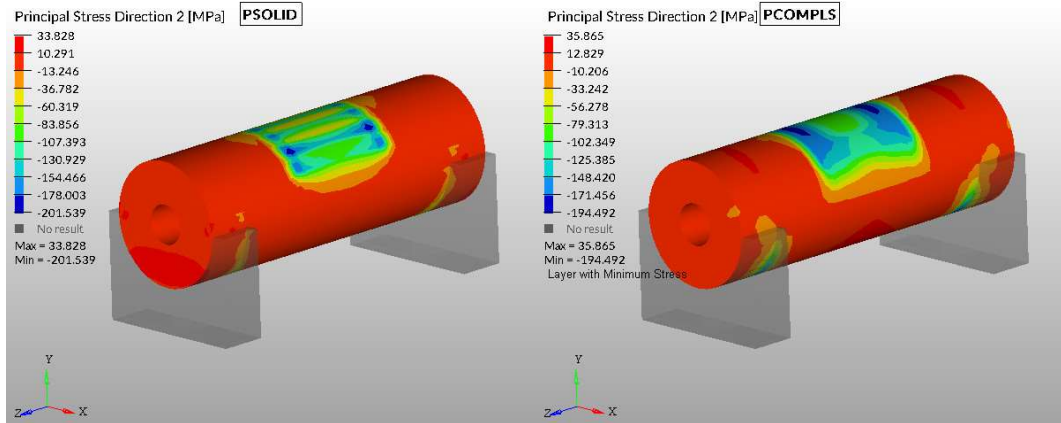


Figure V. 2-38 Principal Stress Direction 2 Comparison Top View

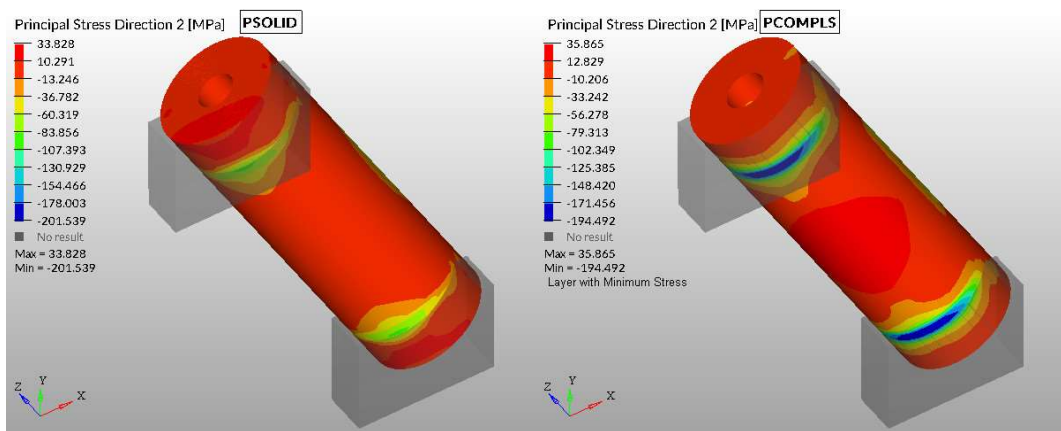


Figure V. 2-39 Principal Stress Direction 2 Comparison Bottom View

The results of the principal stress along transversal directions are very similar between PSOLID and PCOMPLS. The distribution is similar, with a higher maximum compressive stress values in the PCOMPLS around the piston hubs and in the central region (connecting rod).

In both cases the maximum transversal resistance of the material is reached and this could bring to a failure. Considering a transversal compressive resistance  $F_{2c}$  equal to the 80% of the transversal traction resistance  $F_{2t}$ :

$$F_{2c} = 80\% (F_{2t}) = 80\% (-46,7 \text{ MPa}) = -37,36 \text{ MPa}$$

Equation V. 2-2 Transversal Compressive Resistance

### Principal Stress – Direction 3:

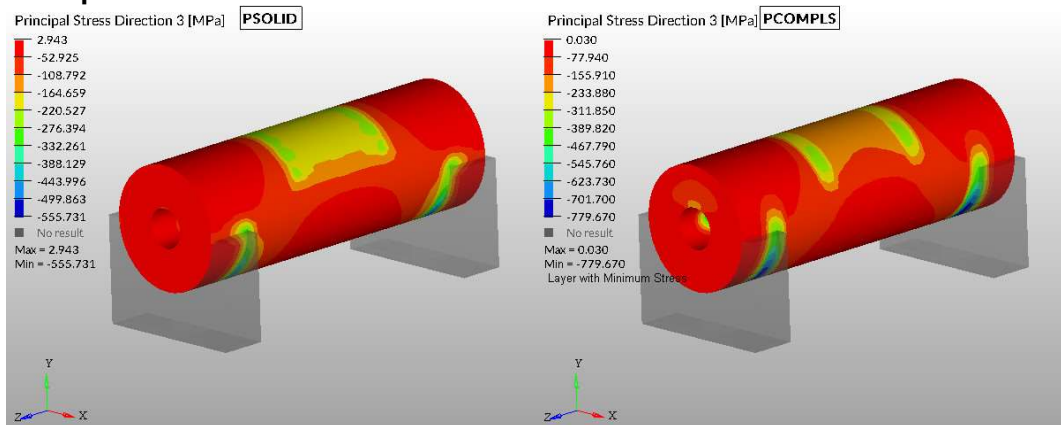


Figure V. 2-40 Principal Stress Direction 3 Comparison Top View

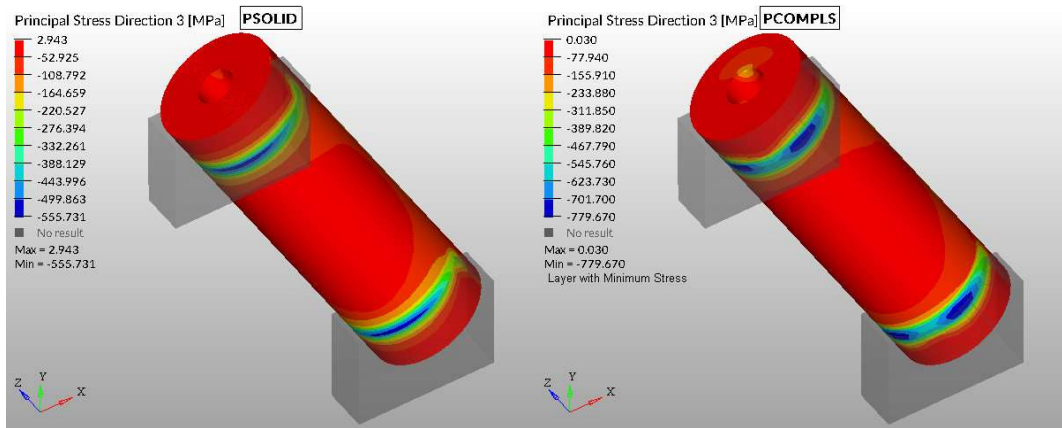


Figure V. 2-41 Principal Stress Direction 3 Comparison Bottom View

The results of the principal stress along transversal directions are very similar between PSOLID and PCOMPLS. The distribution is similar, with a higher maximum compressive stress values in the PCOMPLS around the piston hubs.

**Shear Stress:**

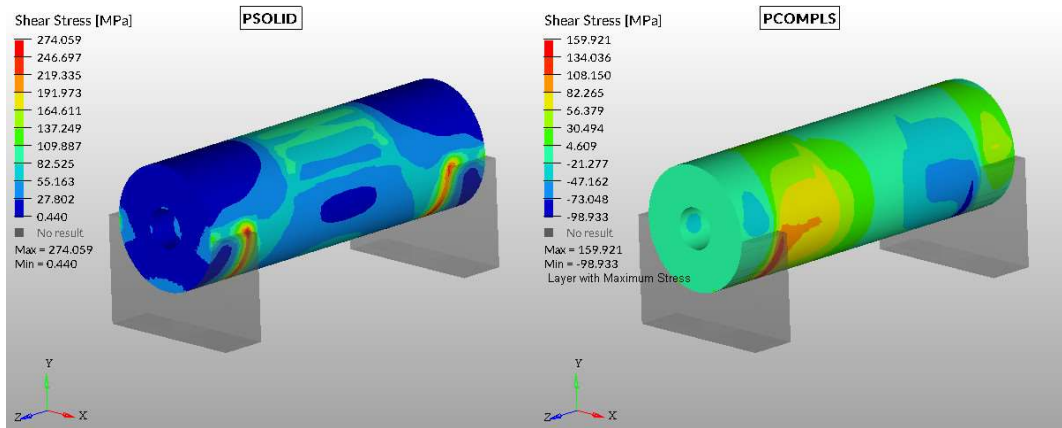


Figure V. 2-42 Shear Stress Comparison Top View

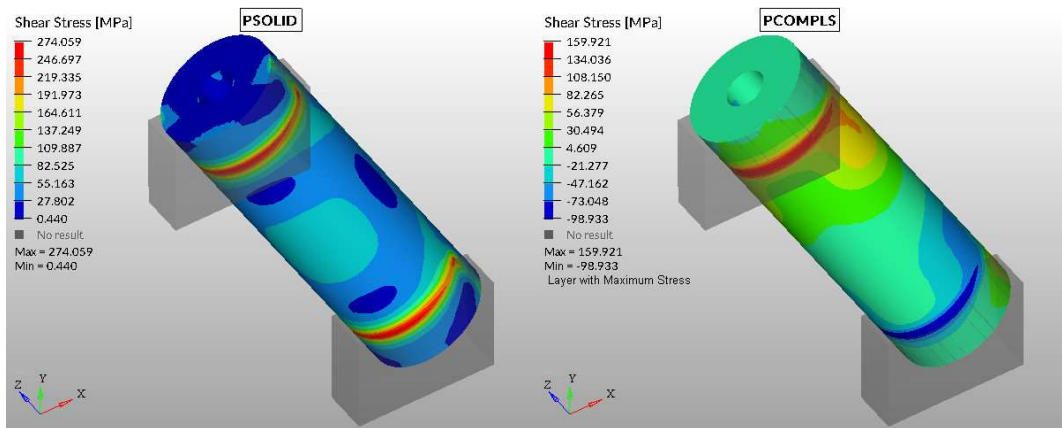


Figure V. 2-43 Shear Stress Comparison Bottom View

This last result show very well the imprecision of the PCOMPLS. The shear stress distribution is not acceptable at all. The values of the stresses are different. This makes the PCOMPLS not reliable in terms of composite material analysis.

Aim of the PSOLID was to verify the effectiveness of the PCOMPLS property. As it was possible to see there are important differences between the two models. This brings to a conclusion about the PCOMPLS. Its potential is very high, but at the actual state of art it is not reliable. The results are acceptable in certain cases and totally different in others.

From all the considerations done in the last paragraphs, it is possible to expect a failure of the wrist pin. Further experiments should be performed to verify the failure of the component. Software implementations should be carried out to have more detail about the stress state and the failure index of the components.

### **V. 3. Future developments**

From the Altair website it was possible to discover that further implementation of the PCOMPLS will be introduced in the next release of the software. The potential of this element is still high, but the lack of a visual validation tool represents a big obstacle. The introduction of a material orientation script in the realization of the PSOLID model helped in the creation of a comparative model.

In terms of meshing process, the use of the PCOMPLS allows to reduce considerably the meshing time, since a single continuous mesh can be used. The layering will be managed directly by the PCOMPLS property. The creation of the layers with the PCOMPLS is fast and easy, but the orientation of the fibers can be only changed by manually modifying the .fem file. This brings to a reduction of the overall analysis efficiency.

In general, it is possible to notice a lack of instrumentation related to the solid layered elements. Even the use of the PSOLID was limited by the impossibility to change the material orientation.

Finally, the failure criterion is completely absent for the solid layered components. This brings to a huge lack of knowledge about the feasibility of the components discussed in this project. Indeed, the component strain and stress are showed correctly, but no hypothesis on failure was done on them.

From an experimental point of view, a thesis focused on composite material UD PES-AS4 tests would be recommended to validate the software results and the mechanical characteristic of the material. It would be appropriate also to evaluate the use of alternative composite material with a better rub resistance, such as the Kevlar. In particular on the layer of the rod and the pin where they are in contact with the bushing. In fact, the oil layer should be always present, but in any case, this solution could give a better safety coefficient.

Regarding the layering method, an optimization of the different plies can be subject of a thesis. This project aim was to introduce the PCOMPLS elements and to lighten an engine component. These objectives were both reached, but future implementations are still required. The orientation of the fibers wasn't optimized, but only chosen after some practical argumentations. The results of this project represent a "launch pad" for future thesis about composite components simulation on Hypermesh and Optistruct.

The lightening of the engine wasn't faced in a complete way. Only the wrist pin and the connecting rod were analyzed. The weight reduction of the wrist pin and of the connecting should be accompanied by a lightening of the other engine components, such as the crankshaft, crank-webs and crank case. This overall lightening would bring to a substantial benefit.

## VI. Bibliography

- [1] Cristiana Delprete, *Powertrain Components Design Didactic Material*. Available: <https://didattica.polito.it/>
- [2] Altair Engineering. Available: <http://www.altair.com>.
- [3] Altair Connect. Available: <https://connect.altair.com/>
- [4] Altair Forum. Available: <https://forum.altair.com/>
- [5] Altair University released: 1st edition 05/2018, Academic Program: *Introduction to Practical Aspects of Composites*
- [6] Shuguang Li, Elena Sitnikova, Yuning Liang, Abdul-Salam Kaddour, August 2017, *The Tsai-Wu failure criterion rationalised in the context of UD composites*, Available: [www.elsevier.com/locate/compositesa](http://www.elsevier.com/locate/compositesa)
- [7] "Six-Sided Solid Element Connection - Figure 2. CHEXA Element R, S, and T Vectors", Available: <https://knowledge.autodesk.com/support/nastran>
- [8] Yijing Li and Jernej Barbic, *Stable Orthotropic Materials*, Editors: Vladlen Koltun and Eftychios Sifakis, Eurographics/ACM SIGGRAPH Symposium on Computer Animation (2014)
- [9] Matteo Conese, *Design of engine components with thermoresistant composite material*, 2019